Structure and Cholesterol Dynamics of Caveolae/Raft and Nonraft Plasma Membrane Domains†

Adalberto M. Gallegos,‡,§ Stephen M. Storey,‡,§ Ann B. Kier,‡ Friedhelm Schroeder,|| and Judith M. Ball*,‡

Department of Pathobiology, Texas A&M University, TVMC, College Station, Texas 77843-4467, and Department of Physiology and Pharmacology, Texas A&M University, TVMC, College Station, Texas 77843-4466

Received February 8, 2006; Revised Manuscript Received August 3, 2006

ABSTRACT: Despite recognition that the plasma membrane (PM) is comprised of lipid raft domains that are key organizing sites of multiple signaling pathways and other cell functions, limited information is available regarding the structure and function in sterol dynamics of these microdomains. To begin to resolve these issues, MDCK membranes were subfractionated by three different techniques to produce (i) detergent-resistant membranes (DRM) and detergent-soluble membranes (DSM), (ii) nondetergent caveolae/rafts (NDCR), and (iii) nondetergent, affinity-purified caveolae/rafts (ACR) and noncaveolae/nonrafts (NR). ACR exhibited the least cross contamination with other PM domains or intracellular membranes, in marked contrast to DRM that contained the highest level of cross contaminants. Spectral properties of dehydroergosterol (DHE), a naturally occurring fluorescent sterol, showed that ACR, NDCR, and NR did not contain crystalline sterol, consistent with the lack of crystalline sterol in PM of intact cells. In contrast, DRM contained significant levels of crystalline sterol. Fluorescence polarization of membrane probes showed that ACR were the least fluid and had the highest transbilayer fluidity gradient, the most liquid ordered phase, and the sterol dynamics most responsive to sterol carrier protein-2 (SCP-2). In contrast, DRM had structural properties similar to those of NR, anomalous (very fast) spontaneous sterol dynamics, and sterol dynamics that were unresponsive to SCP-2. Differences between the structural and functional properties of DRM and those of the nondetergent preparations (ACR and NDCR) were not due to the presence of detergent. A nondetergent, affinity-purified (ACR) lipid domain fraction isolated from MDCK cells for the first time revealed unique structural (noncrystalline sterol, liquid-ordered, high transbilayer fluidity gradient) and functional (cholesterol dynamics) properties of lipid rafts as compared to nonrafts (NR). In summary, this study showed membrane microdomains (rafts/caveolae) isolated by three different methodologies have unique structural, functional, and organizational characteristics.

A growing body of evidence indicates that cholesterol-rich domains/lipid rafts provide a nexus for organizing not only reverse cholesterol transport (*1*, *2*) but also many physiological processes at the plasma membrane (PM),[1] including receptor−effector coupling, signaling, immune function, transcytosis, and cell recognition (reviewed in ref *3*). Cholesterol-rich lipid rafts/caveolae also serve as entry portals for microorganisms, including bacteria (and associated toxins such as cholera toxin, Shiga toxin, and Shiga-like toxin), viruses (for example, Ebola, Marburg, Echovirus, and HIV), and parasites (malaria) (reviewed in ref *3*).

Despite the putative importance of cholesterol-rich domains/lipid rafts in cellular function, their existence in the PM of living cells has only recently been addressed. A variety of techniques using tagged proteins or lipids have been utilized to visualize lipid rafts enriched in the respective markers (reviewed in ref *3*), yet these studies have failed to directly visualize sterol in the PM. Recent studies utilizing real-time multiphoton imaging and pattern distribution analyses of dehydroergosterol (DHE) for the first time detect the existence of sterol-rich and -poor domains/rafts in the PM of living cells (*4*, *5*). Although it is known that DHE is not identical to cholesterol, DHE is a naturally occurring fluorescent sterol (yeast and Red Sea sponge), readily replacing endogenous sterol in cultured cells and exhibiting structural as well as functional properties closely resembling

† This work was supported in part by the U.S. Public Health Service, National Institutes of Health Grants GM63236 (J.M.B.) and GM31651 (F.S. and A.B.K.), and by Mentored Quantitative Research Career Development Award (K25) DK62812 (A.M.G.).

* To whom correspondence should be addressed: Department of Pathobiology, Texas A&M University, TVMC, College Station, TX 77843-4467. Phone: (979) 845-7910. Fax: (979) 845-9231. E-mail: jball@cvm.tamu.edu.

‡ Department of Pathobiology.

§ These authors contributed equally to this work.

|| Department of Physiology and Pharmacology.

[1] Abbreviations: ACR, nondetergent, affinity-purified caveolae/rafts; NDCR, nondetergent caveolae/rafts; NR, noncaveolae/nonrafts; DRM, detergent-resistant membranes; DSM, detergent-soluble membranes; ConA, concanavalin A; SCP-2, sterol carrier protein-2; DHE, dehydroergosterol; DPH, 1,6-diphenyl-1,3,5-hexatriene; DPH-TMA, 1,6-diphenyl-1,3,5-hexatrienyltrimethylammonium; DPH-Pro, 3-(1,6-diphenyl-1,3,5-hexatrienyl)propionic acid; *cis*-parinaric acid, (9*Z*,11*E*,-13*E*,15*Z*)-octatetradecanoic acid; *trans*-parinaric acid, (9*E*,11*E*,13*E*,-15*E*)-octatetradecanoic acid; NBD-stearic acid,12-(*N*-methyl)-*N*-[(7-nitrobenz-2-oxa-1,3-diazol-4-yl)amino]octadecanoic acid; DiI_1,1,1′,3,3,3′,3′-hexamethylindodicarbocyanine iodide; DiI_{18}, 1,1′-dioctadecyl-3,3,3′,3′-tetramethylindocarbocyanine perchlorate; BHT, butylated hydroxytoluene; PBS, phosphate-buffered saline; PM, plasma membrane; ER, endoplasmic reticulum.

10.1021/bi0602720 CCC: $33.50
Published on Web 09/09/2006

those of cholesterol (reviewed in refs *4* and *6*−*16*). Thus, it would appear that cholesterol-rich rafts do exist in living cells and are not just an artifact induced by subcellular fractionation protocols or nonphysiological probe molecules.

Elucidation of the biochemical and structural characteristics of cholesterol-rich lipid rafts also has been difficult. To date, the majority of biochemical characterizations have been performed on detergent-resistant membrane (DRM)-enriched fractions, and concerns about whether DRM equate with lipid rafts as well as whether such domains reflect the biological nature of intact cells remain (reviewed in refs *17*−*19*). Fluorescence probes indicate that the physical state of lipids in DRM isolated from model membranes is in a liquid ordered state, intermediate between the liquid crystalline and gel states (reviewed in refs *3*−*5*). Likewise, fluorescence and electron spin resonance techniques show that the lipids of DRM isolated from cultured cells are also in a liquid ordered state (*20*). Although the liquid ordered state is not due to the presence of detergents within the DRM, detergent extraction itself may induce the formation of the liquid ordered state (reviewed in refs *17* and *18*). Despite the limitations of DRM, however, this approach has focused attention on and significantly contributed to our understanding of lipid rafts, as evidenced by the appearance of a great number of publications using this technique over the past decade. Simultaneous with the development of DRM was the work of other investigators who focused on techniques avoiding the use of detergents (reviewed in refs *3* and *21*), yet very little is known regarding the structural or functional properties of these preparations. To date, only a single report has examined the physical structure of lipids in lipid rafts isolated without the use of detergents (*22*). The latter study showed that lipid rafts isolated from L-cell fibroblasts using a classical nondetergent method (*21*) are in a liquid ordered state. While the physiological significance of these observations to intact cells is not completely clear, a recent study using two-photon microscopy of a synthetic fluorescent molecule (Laurdan) revealed microscopically visible liquid ordered lipid domains in macrophages and fibroblasts in culture (*23*). The size of the liquid ordered domains (183−800 nm) detected in the PM of living cells is in the same range as the size of sterol-rich domains imaged by three-photon microscopy of DHE (*5*).

Despite reports that cholesterol-rich domains have important functions in reverse cholesterol transport (reviewed in refs *2*−*4*), little is known regarding the structure, cholesterol dynamics, and cholesterol responsiveness to intracellular cholesterol binding proteins (e.g., sterol carrier protein-2). To begin to address these questions, MDCK cells were used to isolate four types of lipid domain fractions: DRM obtained with Triton X-100, nondetergent caveolae/rafts (NDCR), nondetergent affinity-purified caveolae/rafts (ACR), and noncaveolae/nonrafts (NR).

MATERIALS AND METHODS

Materials and Marker Antibodies. Cholesterol (>99% pure) and ergosterol (>99% pure) were purchased from Steraloids (Wilmington, NH). EDTA, Tris base, sucrose, phosphate-buffered saline (PBS), PMS-F, and Percoll were obtained from Sigma Chemical (St. Louis, MO). Optiprep was purchased from Accurate Chemical Scientific Corp. (Westbury, NY). Lipid-soluble fluorophores, including 1,6-diphenyl-1,3,5-hexatriene (DPH), 1,6-diphenyl-1,3,5-hexatrienyltrimethylammonium (DPH-TMA), 3-(1,6-diphenyl-1,3,5-hexatrienyl)propionic acid (DPH-Pro), (9*Z*,11*E*,13*E*,15*Z*)-octatetradecanoic acid (*cis*-parinaric acid), (9*E*,11*E*,13*E*,15*E*)-octatetradecanoic acid (*trans*-parinaric acid), 12-(*N*-methyl)-*N*-[(7-nitrobenz-2-oxa-1,3-diazol-4-yl)amino]octadecanoic acid (NBD-stearic acid), 1,1′,3,3,3′,3′-hexamethylindodicarbocyanine iodide (DiI_1), and 1,1′-dioctadecyl-3,3,3′,3′-tetramethylindocarbocyanine perchlorate (DiI_{18}) were obtained from Molecular Probes (Eugene, OR). All solutions in which water was used contained milliQ/deionized water.

Mouse anti-sheep sodium/potassium-ATPase α subunit was obtained from Affinity BioReagents, Inc. (Golden, CO). Rabbit anti-canine calnexin peptide (amino acids 575−593) was purchased from Stressgen Biotechnologies (Victoria, BC). Mouse anti-flotillin-1 peptide (amino acids 312−428) was from BD Transduction Laboratories (Lexington, KY). Both goat anti-rabbit IgG*HRP and goat anti-mouse IgG*HRP antisera were obtained from Southern Biotechnologies Associates, Inc. (Birmingham, AL). Rabbit anti-human caveolin-1 peptide (amino acids 2−31) antibodies were raised in rabbits against a 29-amino acid peptide, deduced from the human caveolin-1 sequence, cross-linked to KLH with glutaraldehyde.

Dehydroergosterol Synthesis. Although dehydroergosterol (DHE) occurs naturally in yeast and Red Sea sponge, DHE utilized herein was chemically synthesized from ergosterol (>99% pure) by a method developed in our laboratory (*4*, *24*). This method yielded DHE with a high degree of purity (>99%), as ascertained by high-performance liquid chromatography (*22*, *25*).

Cell Culture. Madin Darby canine kidney (MDCK, American Type Culture Collection) cells were grown in high-glucose (4.5 g/L) Dulbecco's Modification of Eagle's medium (D-MEM) (Cellgrow/Mediatech, Herndon, VA) supplemented with the following: 2 mM L-glutamine (BioWhittaker/Canbrex, East Rutherford, NJ), 1 mM sodium pyruvate (BioWhittaker/Canbrex), 0.1 mM nonessential amino acids (Cellgrow/Mediatech), 100 units/L penicillin, 100 μg/L streptomycin, and 0.25 μg/L Fungizone (BioWhittaker/Cambrex), 43.9 mM sodium bicarbonate (Gibco/Invitrogen, Carlsbad, CA), and 5% fetal bovine serum and 5% Serum Supreme (BioWhittaker/Cambrex). Cell stocks, maintained in 175 cm^2 flasks (Sarstedt, Newton, NC), were expanded into 500 cm^2 trays and grown to 85% confluence for membrane isolations.

Cell Culture for Bioincorporation of Fluorescent Sterol (DHE). For measurement of fluorescent sterol dynamics in purified membrane fractions (see below), MDCK cells were cultured with equivalent amounts of DHE to produce donor membrane fractions, as described previously for other cell lines (*4*, *10*, *26*). Since DHE supplementation does not alter the sterol content of the membrane fractions (*10*, *26*), this ensured that the exchange assay determined sterol exchange, rather than net transfer down a concentration gradient. Briefly, to prepare fluorescent sterol-containing donor membrane fractions for sterol exchange assays, the MDCK cells were cultured as described above for 72 h, the medium was removed, and the cells were washed with PBS, followed by the addition of serum-free medium containing DHE (20 μg/mL serum-free medium). DHE was freshly prepared as a

concentrated stock solution in 95% ethanol containing 1 mol % butylated hydroxytoluene (BHT) and stored at −80 °C. DHE was then added to the serum-free culture medium (20 μg/mL serum-free medium) so that the final concentration of ethanol was <0.3%. Since cells rapidly metabolize ethanol and cells were incubated with the DHE for 18 h, the low level of ethanol (<0.3%) initially added to the culture medium had no effect on cell growth, membrane cholesterol distribution, or membrane biochemical properties (*10*). Acceptor membrane fractions were obtained similarly except that the MDCK cells were cultured in serum-free maintenance medium without DHE. At the end of an 18 h culture, the cells were subjected to subcellular fractionation techniques described below.

Isolation of Detergent-Resistant Membranes (DRM) and Detergent-Soluble Membranes (DSM) from MDCK Cells. DRM and DSM were isolated from MDCK cells as previously described for other polarized cell lines (*27*). Cultures were washed twice in PBS, scraped twice with 2 mL (4 mL final volume) of TNE buffer [20 mM Tris-HCl (pH 7.4), 150 mM NaCl, 1 mM EDTA, 0.2 μM PMS-F, and 1% Triton X-100], and passed 10 times through a 22-gauge needle. The resulting homogenate was incubated at 4 °C for 30 min and mixed with 2.5 M sucrose to a density of 40% as part of a discontinuous sucrose density gradient (40% → 35% → 5%). After ultracentrifugation at 180000*g* and 4 °C for 18 h with an SW41Ti rotor and Optima LE-80k ultracentrifuge (Beckman Instruments, Fullerton, CA), DRM were recovered from the 35%−5% interface. For Western blot analysis and the sterol exchange assay, the DRM (35%−5% interface) and Triton X-100 soluble material, termed DSM (40% gradient layer), were further processed by ultracentrifugation (190000*g* for 1.5 h in a Beckman SW41Ti rotor) in Tris buffer (10 mM Tris and 1 mM EDTA) and suspended in PBS for protein quantification (Pierce Micro BCA assay) or in PBS containing 0.2 μM PMS-F and 1 μL/mL protease inhibitor cocktail set III (Calbiochem) for storage at −80 °C. The final purified DRM and DSM were aliquoted in 3.5 μg protein aliquots for donors and 35 μg protein quantities for acceptors.

Isolation of Nondetergent Caveolae/Raft Domains (NDCR) from Purified Plasma Membrane Vesicles Isolated from MDCK Cells. First described by Smart et al. (*21*), this procedure utilizes differential (Percoll) centrifugation to first isolate purified PM, followed by subfractionation of the PM vesicles on OptiPrep density gradients. The originally reported method was modified by first culturing MDCK cells with and without DHE as described above and isolated as follows. Four 500 cm^2 trays of MDCK cells cultured with the respective sterols were grown to a density of approximately 6×10^7 cells per tray (∼85% confluency), washed twice with PBS, scraped twice with 4 mL (8 mL final volume) of PBS containing 0.2 μM PMS-F, and sedimented by ultracentrifugation at 1000*g* and room temperature (RT) for 5 min in a model GR4.11 Jouan centrifuge (Jouan, SA, Cedex, France). The cells were suspended in 2 mL of ice-cold 0.25 M sucrose, 1 mM EDTA, and 20 mM Tris-base (pH 7.8) and sonicated on ice with a cuphorn for four 30 s bursts at 30 s intervals (Misonix 3000, Misonix Inc., Farmingdale, NY) set to power level 3. The nuclei were sedimented at 1000*g* and RT for 10 min. The resulting postnuclear supernatant (PNS) was layered onto 30% Percoll (Amersham Biosciences Corp., Piscataway, NJ) and centrifuged at 84000*g* for 30 min at 4 °C in a Beckman SW41Ti rotor. The opaque protein band near the middle of the gradient (PM-enriched fraction) was removed (∼2 mL total volume) and sonicated on ice with six 30 s bursts at 30 s intervals on ice with a cuphorn (Misonix, Inc.). The PM-enriched fraction was diluted with 50% (weight per volume) OptiPrep to a final concentration of 23% OptiPrep. A continuous gradient of 10 and 20% OptiPrep (1:1, v/v) was layered onto the membrane fraction, and the procedure was continued exactly as described previously (*21*). Then, 0.2 μM PMS-F and 1 μL/mL protease inhibitor cocktail set III were added to the nondetergent caveolae/rafts (NDCR) before storage at −80 °C in aliquots of 3.5 μg protein quantities for donors (i.e., containing DHE) and 35 μg quantities for acceptors (lacking DHE).

Isolation of Concanavalin A Affinity-Purified Caveolae/Raft Domains (ACR) and Noncaveolae/Nonraft Domains (NR) from Purified Plasma Membrane Vesicles Isolated from MDCK Cells. PM-derived affinity-purified caveolae/rafts (ACR) and noncaveolae/nonrafts were isolated using a modification of a previously established concanavalin A-based affinity method (*1*, *18*, *25*). All centrifugation steps utilized a Beckman SW41Ti rotor and Optima LE-80k ultracentrifuge. PM was first isolated by sucrose gradient centrifugation for the removal of intracellular contaminants, followed by concanavalin A-based affinity chromatography of PM vesicles to yield ACR and NR. Briefly, MDCK cells cultured in 500 cm^2 trays with or without DHE were pelleted as described above. The cells were suspended in 2 mL of 0.25 M sucrose, 1 mM EDTA, and 20 mM Tris base (pH 7.8) and homogenized by nitrogen gas cavitation (15 min at 40 psi), and the nuclei were removed by centrifugation as described above. The resulting PNS was floated on a discontinuous sucrose density gradient (0.5 mL at 55%, 1.5 mL at 40%, 1.5 mL at 35%, 1.5 mL at 32%, 1.5 mL at 29%, 1.5 mL at 27%, 1.5 mL at 20%, and 0.5 mL at 8.3%; w/v in Tris buffer) and centrifuged at 192000*g* and 4 °C for 90 min. The PM fractions at the 27%−29% and 29%−32% interfaces were sonicated on ice with three 1 s bursts at 10 s intervals using a Misonix Sonicator 3000 with a cuphorn and then added to a concanavalin A−Sepharose 4B slurry (equivalent to 25 mL of preswollen 4B material; 10−16 mg of ConA/mL of drained medium) in buffer A [0.14 M KCl, 0.01 M HEPES, 1 mM $MgCl_2$, and 1 mM $MnCl_2$ (pH 7.8) with KOH]. The sample slurry was mixed by lightly bubbling nitrogen through the solution for 2 min, incubated for 10 min at RT for binding, then transferred to a glass preparative column, and allowed to settle for 15 min. The flow-through was collected in 14 mL increments and centrifuged at 111000*g* and 4 °C for 14 h, and the resulting noncaveolae/nonraft (NR) protein pellets were suspended in small volumes of buffer A for protein quantification by BCA. After an additional wash with 25 mL of buffer A, 14 mL volumes of buffer B (0.5 M methyl mannosidase in buffer A) were added to the column and mixed with nitrogen bubbling for 10 min. Six volumes of buffer B were collected and centrifuged at 111000*g* and 4 °C for 14 h, and the resulting ACR protein pellets were suspended in small volumes of buffer A for protein quantification or buffer A containing 0.2 μM PMS-F and 1 μL/mL protease inhibitor cocktail set III for storage at −80 °C as described above.

Western Blotting To Determine the Purity of Purified Membrane Fractions. A series of Western blots were used to detect the presence of specific markers for PM domains or intracellular organelles (e.g., endoplasmic reticulum). Protein concentrations were calculated from a BSA standard curve of absorbance at 280 nm with a Cary100 UV−visible spectrophotometer (Varian, Palo Alto, CA), and then 5 μg (per lane) of total protein from each fraction was resolved by 12% SDS−PAGE and electroblotted onto nitrocellulose filters (GE Osmonics Inc., Minnetouka, MN). The filters were blocked in 10% weight per volume nonfat dry milk in PBS (10% blotto) for 1 h at RT and blotted with the primary antibody (1° Ab) in 2.5% blotto for 14 h at 4 °C. Reactive bands were visualized by the addition of horseradish peroxidase (HRP)-conjugated IgG and SuperSignal West Pico chemiluminescent substrate (Pierce) followed by exposure to Kodak X-OMAT film (*28*).

Incorporation of Fluorescent Probes for Measurement of Fluorescence Polarization in Purified Membrane Fractions. All fluorophores were prepared as stock solutions in 200 proof anhydrous ethanol with 2 wt %/volume butylated hydroxytoluene as an antioxidant. The fluorescent probes were DHE, DiI_{18}, DiI_1, *trans*-parinaric acid, *cis*-parinaric acid, NBD-stearic acid, diphenylhexatriene (DPH), DPH-TMA, and DPH-propionic acid. DHE was bioincorporated into MDCK cells prior to isolation of purified membrane fractions basically as described in the preceding sections, except that the DHE concentration was 10-fold lower than that used for sterol exchange assays to avoid self-quenching. All other fluorescence probes were directly incorporated into purified membrane fractions. In brief, purified stock membrane fractions from several isolations were pooled together, then washed two times with 10 mM Tris buffer (pH 7.4), and subjected to centrifugation at 30,000 rpm for 45 min at 4 °C in an SW40Ti rotor in an XL90 ultracentrifuge (Beckman Instruments). Fluorescent probes were incorporated into purified membrane fractions by first placing 35 μg of protein of the respective membrane fraction (acceptor, i.e., not containing DHE) in 2 mL of 10 mM PIPES buffer (pH 7.4). Fluorescent probes were added at a ratio of 1000 μg of protein per 1 μg of fluorophore such that final ethanol concentrations were kept at <25 mM. Ethanol concentrations of <25 mM have no effect on membrane structure (*29*, *30*) or interaction of lipid binding proteins with ligands (*31*). Finally, such small amounts of ethanol fail to induce fluorescent sterol self-aggregation and formation of crystalline sterol in lipid rafts either in vitro or in intact cells (*4*). After incubation for 30 min at RT to ensure maximal probe incorporation, fluorescence polarization data were acquired as described below.

Assessment of Membrane and Detergent Buffer by Absorbance Spectroscopy. All absorbance measurements to determine detergent concentrations and protein levels were performed using a Cary 100 Scan UV−visible spectrophotometer (Varian). The spectrophotometer has a sample and reference channel; 2 mL samples were measured in 2 cm quartz cuvettes (Fisher Scientific, Pittsburgh, PA). For measurements involving membranes, 10 mM PIPES buffer was used as a reference.

Assessment of the Steady-State Fluorescence Polarization in Purified Membrane Fractions. All measurements of steady-state fluorescence polarization were taken using a PC1 spectrofluorometer with photon-counting electronics (ISS Instruments, Inc., Champaign, IL) exactly as described previously (*22*). Any residual light scatter contribution to the polarization data with the membrane fractions was corrected by converting polarization to anisotropy according to the relation $r = 2P/(3 - P)$ and subtracting the residual fluorescence anisotropy from all experimental data. To prevent artifacts due to inner filter effects, the absorbance of sample solutions at the excitation wavelengths was kept below 0.15. While we recognize that polarization and anisotropy measurements are comprised of both static (limiting anisotropy) and dynamic (rotational rate) parameters, earlier studies from our laboratories showed that agents which fluidize membranes (ethanol and anesthetics) primarily alter the static (i.e., limiting anisotropy), but not dynamic (rotational), components of polarization and anisotropy measurements (*29*, *30*, *32*−*35*). Since alterations in limiting anisotropy are a measure of the cone angle of fluorescence probe rotation in lipid bilayers, limiting anisotropy and, consequently, polarization of the above probe molecules (at very low, non-self-quenching concentrations) are useful as relative measures of membrane "fluidity".

Assessment of Membrane Sterol Exchange: Release of DHE from the Self-Quenching Fluorescence Polarization Assay. Sterol exchange between the isolated membrane fractions was assessed by using a fluorescent sterol (DHE) exchange assay previously developed by our laboratory (*36*). DHE was used as a probe for cholesterol transfer because it (i) is a naturally occurring fluorescent sterol, (ii) is a close structural analogue of cholesterol, (iii) exhibits the same exchange kinetics as cholesterol in both model membranes and biological membranes, (iv) is taken up by cultured L-cells such that >80% of endogenous sterol is replaced by DHE without altering membrane lipid composition or sterol-sensitive enzymes, (v) is codistributed with cholesterol in model and biological membranes, and (vi) is nontoxic to cultured cells or animals (reviewed in refs *4*, *6*−*16*, and *36*). The underlying premise of the DHE exchange assay is that fluorescence self-quenching of DHE occurs in the donor membrane, which contains high levels of DHE. This results in low DHE fluorescence polarization values for the donor. However, upon addition of a 10-fold excess of acceptor membranes, the donor membrane DHE exchanges sterols one for one with acceptor membranes, thereby resulting in release from self-quenching of DHE. This results in an increase in DHE polarization.

In all sterol exchanges, DHE fluorescence polarization of the donor membrane fraction sample was assessed for 20 min in 2 mL of 10 mM PIPES buffer to ensure a stable signal baseline and to obtain an initial value for the fluorescence polarization. This was followed by addition of a 10-fold excess of acceptor (i.e., no DHE) membrane. The protein concentration of the donor membrane fractions was 1.5 μg/mL in 10 mM PIPES buffer (2 mL total volume), whereas the protein concentration of the acceptor membrane fraction was 15.0 μg/mL in the 2 mL sample. The DHE polarization was subsequently recorded during 20 s intervals for 3 or 4 h to monitor sterol transfer between membranes.

Standard Curves for the Sterol Exchange Assay. We note that DRM (*37*, *38*), NDCR (*21*, *22*, *37*, *38*), and ACR (*25*) obtained from all three isolation methods are relatively lipid-rich, and cholesterol-rich compared to the PM. Also, the

sterol/phospholipid ratio in caveolae/raft domains isolated by detergent-free methods (*4*, *37*, *38*) is basically similar to that of PM (*37*, *39*). The standard curve that calculates the fraction of DHE remaining in the donor membrane fraction during an exchange is a polynomial equation involving polarization P of the exchange in the form of

$$P = \sum b_n X_d^{\,n} \quad (1)$$

where X_d is the mole fraction of DHE left in the donor.

For sterol exchange between the donor membrane fraction and the acceptor membrane fraction, a polynomial with two terms yielded a fit with an r^2 of 0.9999 (i.e., eq 2):

$$P(x) = b_0 + b_1 X_d + b_2 X_d^{\,2} \quad (2)$$

where $b_0 = 0.3261$, $b_1 = 0.016$, and $b_2 = -0.144$.

Calculation of the Initial Rate of Sterol Transfer. The initial rate of DHE exchange between donor and acceptor membrane fractions was estimated from the first 10 min of exchange data by using the standard curve described above in eq 2 (*39*). In essence, eq 2 is the definitive relation that describes the exchange between donor and acceptor membranes. Taking the time derivative of eq 2 yields

$$dP/dt = b_1(dX_d/dt) + 2b_2X_d(dX_d/dt) \quad (3)$$

As $t \rightarrow 0$, $X_d \rightarrow 1$ (i.e., initial rate criteria), and if eq 3 is rearranged, the following expression is obtained:

$$(1/(b_1 + 2b_2)) \times (dP/dt)|_{t\rightarrow 0} = (dX_d/dt)|_{t\rightarrow 0} \quad (4)$$

To obtain the molar transfer rate of DHE (d[DHE]/dt) from the donor membrane fraction to the acceptor membrane fraction, dX_d/dt was transformed into d[DHE]/dt by factoring in the initial donor membrane fraction protein concentration (1.5 μg of protein/mL), the total sterol-to-protein concentration in the donor membrane fraction (1011.02 pmol of total sterol/μg of protein), and the values of b_1 (0.016) and b_2 (-0.144). Combining this information with eq 4 yielded eq 5:

$$(d[DHE]/dt)|_{t\rightarrow 0} = -2253 \text{ pmol} \times (dP/dt)|_{t\rightarrow 0} \quad (5)$$

The initial rate of DHE transfer was directly estimated by substituting the initial measured rate of fluorescence polarization change per unit time (i.e., minutes) for $(dP/dt)|_{t\rightarrow 0}$.

Calculation of the Kinetic Parameters of Sterol Exchange. The kinetic parameters of exchange between membrane fraction donor−acceptor pairs were determined by use of the standard curve equation, i.e., eq 2, and the equation for a one-exponential exchange:

$$X = f_1 \exp(-kt) + f_2 \quad (6)$$

where f_1 and f_2 are the exchangeable and nonexchangeable fractions, respectively, of the sterol in the exchange assay and k is the rate constant of the exchange. The expression for X in eq 6 was substituted into eq 2 to produce the expression describing the exchange:

$$P(x) = b_0 + b_1[f_1 \exp(-kt) + f_2] + b_2[f_1 \exp(-kt) + f_2]^2 \quad (7)$$

The exchange curves were fit to eq 8 with r^2 values varying from 0.97 to 0.99. The half-time, $t_{1/2}$, of the exchanges was defined by the following equation:

$$t_{1/2} = (\ln 2)/k \quad (8)$$

Data and Statistical Analyses. All curve fitting and data analyses herein were performed by using SigmaPlot (Jandel Scientific, San Rafael, CA) scientific data analysis and graphing software.

RESULTS

Purification of Caveolae/Raft-Enriched Plasma Membrane Fractions: Detergent-Resistant Membranes (DRM), Nondetergent Caveolae/Raft Domains (NDCR), and Affinity-Purified Caveolae/Raft Domains (ACR). Western blotting and densitometric analysis of DRM (Figure 1A, top row) indicated that the DRM (lane 3) were enriched nearly 10- and 4.3-fold in caveolin-1, a caveolae/raft marker, as compared to MDCK cell homogenate (lane 1) and detergent-soluble membranes (DSM, lane 2), respectively. The DRM fraction exhibited a low level of contamination with calnexin (Figure 1C, top row), which was reduced 2.5- and 1.6-fold (lane 3) as compared to that in the MDCK cell homogenate (lane 1) and DSM fraction (lane 2), respectively. In contrast, DRM were slightly enriched 1.2-fold in the NR marker Na^+/K^+-ATPase (Figure 1B, top row) as compared to MDCK cell homogenate (lane 1) and enriched nearly 10-fold when compared to DSM (lane 2). Thus, although DRM appeared to be enriched in caveolae/raft marker, they also contained endoplasmic reticulum (ER) contaminant and essentially no diminution of the NR PM domain marker.

DSM (Figure 1A, top row, lane 2) contained 4.3-fold less caveolin-1 than the DRM fraction isolated from MDCK cells (lane 3). The DSM fraction had 1.6-fold less ER marker calnexin (Figure 1C, top row, lane 2) than the MDCK cell homogenate (lane 1). However, DSM contained 8- and 10-fold less NR marker Na^+/K^+-ATPase (Figure 1B, top row, lane 2) than the MDCK cell homogenate (lane 1) and DRM (lane 3). Thus, DSM appeared to be depleted of caveolae/raft marker as compared to DRM, but they had also lost the NR marker Na^+/K^+-ATPase.

Western blotting and densitometric analysis indicated that NDCR (Figure 1A, middle row) were enriched 1.4-fold in caveolin-1 as compared to MDCK cell homogenate (lane 1). As confirmation, dot blotting and densitometric analyses showed that NDCR (Figure 1D, middle row) were enriched 1.9-fold in GM1 as compared to MDCK cell homogenate (lane 1). However, the response to anti-calnexin antisera (Figure 1C, middle row) indicated essentially the same content of this ER marker in NDCR (lane 3) as in MDCK cell homogenate (lane 1). Finally, the anti-Na^+/K^+-ATPase marker (Figure 1B, middle row) was enriched 3.7- and 3.7-fold in NDCR domains (lane 3) as compared to MDCK cell homogenate (lane 1) and unfractionated PM (lane 2), respectively. Thus, the NDCR were enriched in the caveolae/raft marker but exhibited no reduction in the level of ER contaminant or NR marker as compared to the unfractionated PM or cell homogenate.

Western blotting and densitometric analysis of caveolae/rafts isolated by use of the detergent-free concanavalin A−Sepharose affinity chromatography (i.e., ACR) revealed

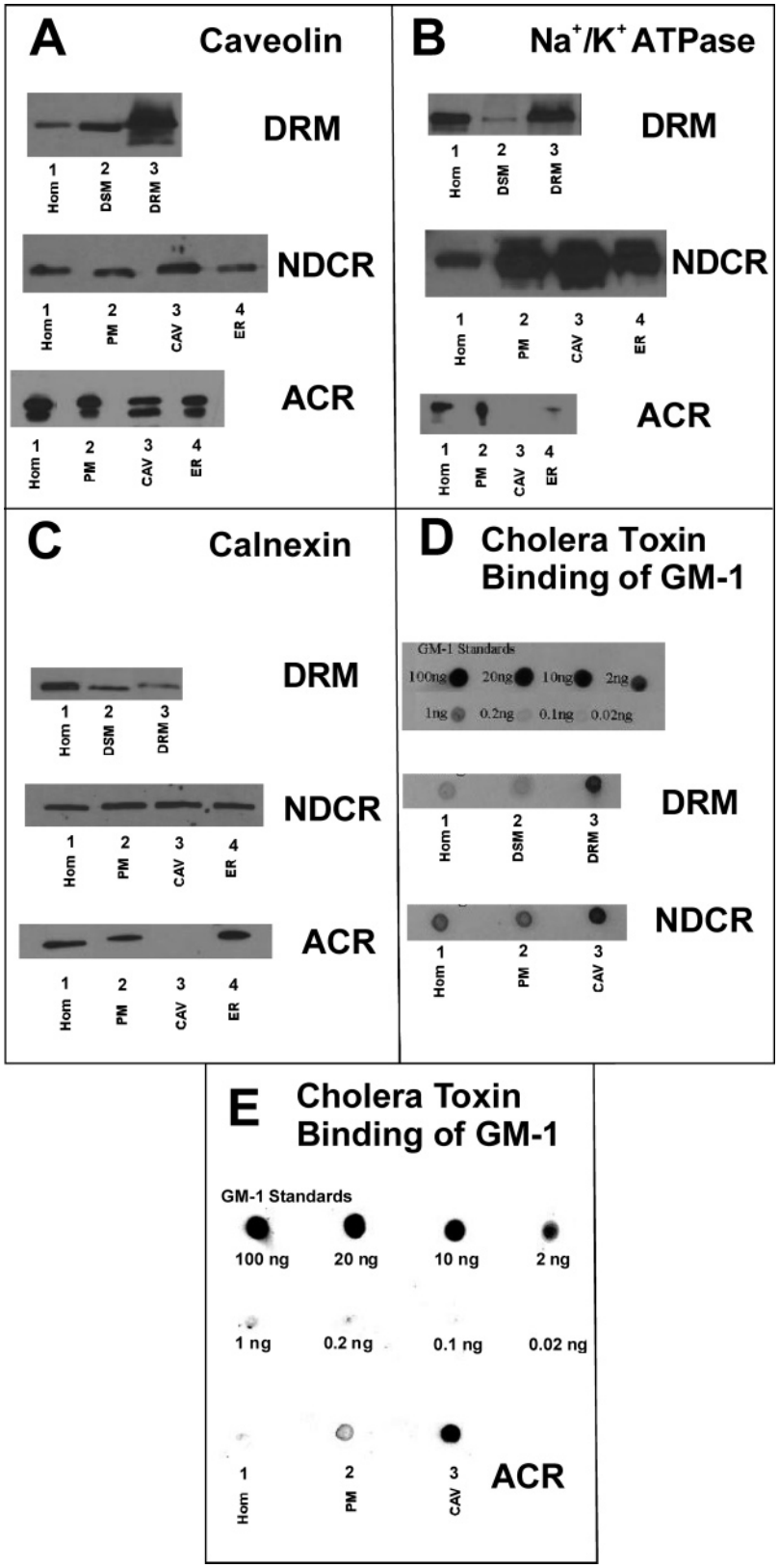

FIGURE 1: Western blotting of protein markers in caveolae/lipid raft preparations. (A) Immunoblot probed with anti-caveolin-1, a marker for caveolae. (B) Immunoblot probed with anti-Na^+/K^+-ATPase, a noncaveolae/nonraft marker. (C) Immunoblot probed with anti-calnexin, an endoplasmic reticulum marker. (D) Dot blot probed with anti-GM1, a caveolae marker. The GM-1 standards for DRM and nondetergent caveolae/rafts are the same. The curve fit of the standards yielded an r^2 of 0.995. (E) Dot blot probed with anti-GM1, a caveolae marker. The GM-1 standards are for affinity-purified caveolae/rafts. The curve fit of the standards resulted in an r^2 of 0.995. Except for panels D and E, in each panel the top row is as follows: lane 1, cell homogenate (5 μg); lane 2, detergent-soluble membranes, DSM (5 μg); and lane 3, detergent-resistant membranes, DRM (5 μg). The middle row is as follows: lane 1, cell homogenate (5 μg); lane 2, PM (5 μg); lane 3, nondetergent caveolae/rafts (5 μg); and lane 4, ER (5 μg). The bottom row is as follows: lane 1, cell homogenate (5 μg); lane 2, PM (5 μg); lane 3, affinity-purified caveolae/rafts (5 μg); and lane 4, ER (5μg).

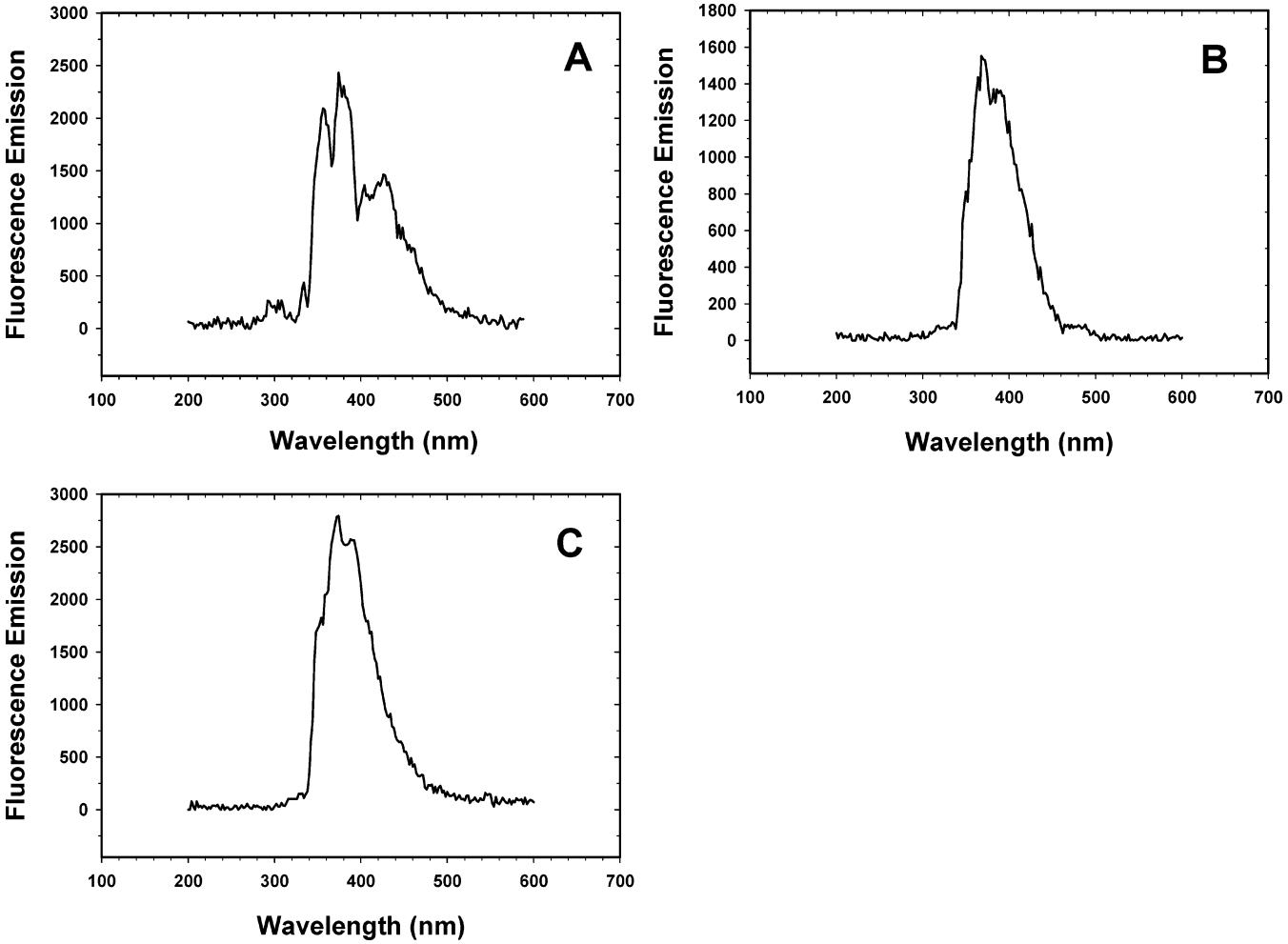

FIGURE 2: Fluorescence emission spectra of dehydroergosterol (DHE) in DRM and caveolae/raft-enriched fractions. (A) Emission spectrum of DRM in PIPES buffer (3.5 μg/2 mL). The excitation wavelength was set to 320 nm. (B) Emission spectrum of nondetergent caveolae/lipid rafts in PIPES buffer (3.5 μg/2 mL). The excitation wavelength was set to 324 nm. (C) Emission spectrum of affinity-purified caveolae/lipid rafts in PIPES buffer (3.5 μg/2 mL). The excitation wavelength was set to 324 nm.

a caveolae/raft-enriched fraction. Anti-caveolin-1 Western blotting (Figure 1A, bottom row) detected caveolin-1 in the ACR isolated from MDCK cells (lane 4). While this was congruent with the ACR fraction being caveolae/rafts, the ACR were not specifically enriched in caveolin-1, most likely due to the presence of large amounts of caveolin-1 in other cellular compartments (e.g., cytoplasmic chaperone complexes, etc.). In contrast, anti-GM1 dot blotting (Figure 1E) showed that the ACR isolated from MDCK cells were enriched ~2.7-fold in GM1 (lane 3). In contrast, the ER marker, calnexin (Figure 1C, bottom row, lane 3), and the NR PM domain marker, Na^+/K^+-ATPase (Figure 1B, bottom row, lane 3), were not detectable in the ACR. Thus, the ACR contained inappropriate caveolae/lipid raft markers and, in contrast to DRM and NDCR, had significantly reduced levels in ER and noncaveolae/nonraft PM markers.

In summary, Western blotting and dot blotting of protein markers indicated that the ACR fraction contained the appropriate caveolae/raft markers while concomitantly being lowest in nonraft markers of any fraction that was examined.

Sterol Structural Properties in Caveolae/Raft-Enriched Membrane Fractions (DHE). We and others have shown that DRM (*37*, *38*), NDCR (*21*, *22*, *37*, *38*), and ACR (*25*) are highly enriched in cholesterol. Although model membrane studies suggest that at such high cholesterol contents the cholesterol may separate into a crystalline phase (reviewed in ref *4*), little is known with regard to the structural phase properties of the cholesterol within DRM or the nondetergent isolates of caveolae/raft domains. Therefore, the fluorescence emission spectral differences in the monomeric (maxima near 356 and 375 nm) versus crystalline (maxima near 403 and 426 nm) DHE phase (*4*) were used to determine structural properties of sterol in DRM, NDCR, and ACR. The fluorescence emission spectra of DHE in DRM exhibit highest intensity maxima near 356 and 375 nm, consistent with the presence of monomeric DHE (Figure 2A). However, additional maxima with approximately half the intensity are noted in the range of 400-453 nm, indicating the presence of significant amounts of DHE in the crystalline phase in DRM (Figure 2A). Taking into account the relative differences in quantum yield, we calculated the proportion of crystalline DHE as described previously (*4*), showing that 7−10% of the sterol within the DRM was in the crystalline state while 90−93% was in the monomeric state. In contrast, the spectra of DHE in NDCR (Figure 2B) and ACR (Figure 2C) exhibited only the emission maxima consistent with the presence of monomeric sterol with no detectable crystalline sterol.

To determine the relative fluidity of the microenvironment wherein the sterol resided in DRM, NDCR, and ACR, the

Table 1: Structural Parameters of Lipidic Probes that Are Preferentially Distributed in Caveolae/Raft Domains, Dehydroergosterol (DHE) and DiI_{18}[a]

membrane	polarization
DHE	
DRM	0.3120 ± 0.0011^{b}
nondetergent caveolae/rafts	$0.3343 \pm 0.0021^{b,c}$
affinity-purified caveolae/rafts	$0.3472 \pm 0.0019^{b,c}$
noncaveolae/nonrafts	0.3078 ± 0.0041^{c}
DiI_{18}	
DRM	0.3381 ± 0.0032^{b}
nondetergent caveolae/rafts	$0.3428 \pm 0.0040^{b,c}$
affinity-purified caveolae/rafts	$0.3479 \pm 0.0029^{b,c}$
noncaveolae/nonrafts	0.3257 ± 0.0053^{c}
DiI_1	
DRM	0.3379 ± 0.0023^{b}
nondetergent caveolae/rafts	0.3397 ± 0.0017^{b}
affinity-purified caveolae/rafts	$0.3466 \pm 0.0037^{b,c}$
noncaveolae/nonrafts	0.3255 ± 0.0046^{c}

[a] DHE, DiI_1, and DiI_{18} were incorporated at low, non-self-quenching levels into purified PM and caveolae/raft domains as described in Materials and Methods. Fluorescence polarization values represent the means ± the standard deviation ($n = 7$). [b] $p < 0.05$ vs noncaveolae/nonrafts. [c] $p < 0.05$ vs DRM.

Table 2: Lateral Structure of Caveolae/Raft Domains and Plasma Membrane Determined by Selectively Probing "Solid" versus "Fluid" Domains with Trans and Cis Fatty Acids[a]

membrane	polarization
trans-parinaric acid	
DRM	0.3267 ± 0.0036
nondetergent caveolae/rafts	$0.3398 \pm 0.0016^{b,c}$
affinity-purified caveolae/rafts	$0.3416 \pm 0.0019^{b,c}$
noncaveolae/nonrafts	0.3245 ± 0.0022
cis-parinaric acid	
DRM	0.3076 ± 0.0014^{c}
nondetergent caveolae/rafts	$0.3201 \pm 0.0016^{b,c}$
affinity-purified caveolae/rafts	$0.3429 \pm 0.0013^{b,c}$
noncaveolae/nonrafts	0.3021 ± 0.0044^{b}
NBD-stearic acid	
DRM	0.3199 ± 0.0025^{c}
nondetergent caveolae/rafts	0.3225 ± 0.0027
affinity-purified caveolae/rafts	$0.3392 \pm 0.0017^{b,c}$
noncaveolae/nonrafts	0.3287 ± 0.0031^{b}

[a] *trans*-Parinaric acid, *cis*-parinaric acid, and NBD-stearic acid were incorporated at low, non-self-quenching levels into purified PM and caveolae/raft domains as described in Materials and Methods. Relative fluorescence polarization values represent the means ± the standard deviation ($n = 7$). [b] $p < 0.05$ vs DRM. [c] $p < 0.05$ vs noncaveolae/nonrafts.

fluorescence polarization of DHE (present at a low, non-self-quenching concentration) was assessed. The fluorescence polarization of DHE in DRM was 0.3120 ± 0.0011, significantly ($p < 0.05$) lower than that of DHE in NDCR and ACR (Table 1). In contrast, the fluorescence polarizations of DHE in DRM, NDCR, and ACR were all significantly higher than in NR.

These data indicated the bulk of DRM sterols are present in a mobile, less ordered microenvironment in spite of the presence of significant amounts (7−10%) of crystalline sterol. Further, the rank order of DHE fluorescence polarization was as follows: ACR (most rigid) > NDCR > DRM > NR (most fluid). Since "mobility" is inversely proportional to polarization, the sterol mobility was lowest not in the DRM but in the preparations not utilizing detergents, in particular, ACR. In summary, these data showed that sterol organization of caveolae/lipid rafts is highly dependent on the method of isolation.

Fluorescence Polarization of Other Lipidic Probe Molecules that Preferentially Localize in Lipid Rafts (DiI_{18} versus DiI_1). To confirm whether the higher fluidity sensed by DHE in DRM was unique to this probe, fluorescence polarization studies were performed with DiI probes, in particular, DiI_{18}, which partitions preferentially into lipid rafts (*40*). The fluorescence polarization of the long alkyl chain length DiI_{18} exhibited the following order of fluorescence polarization: ACR > NDCR > DRM > NR (Table 1). Thus, while the fluorescence polarization of the long alkyl chain length DiI_{18} was significantly higher in DRM than in NR, it was nevertheless significantly lower than that of either of the other lipid raft preparations, i.e., NDCR or ACR (Table 1). Unlike DiI_{18}, which is anchored deep in the bilayer, the short alkyl chain DiI_1 is anchored close to the phospholipid head group−water interface and does not exhibit a preference for lipid rafts versus nonraft domains in lipid bilayers (*40*). Nevertheless, the overall pattern of DiI_1 fluorescence polarization in the membrane fractions was basically similar to that of DiI_{18} (Table 1).

Taken together, both the lipid raft selective DiI_{18} and the nonselective DiI_1 indicated that the acyl chain environments (both deep in the bilayer and closer to the surface, respectively) of the PM ACR domains was the most rigid while the NR domains were the most fluid, with the DRM and other nondetergent caveolae/raft preparations being intermediate. This pattern was very similar to that exhibited by DHE in the various membrane domain preparations shown in the preceding section. Thus, the highest polarization/rigidity obtained was characteristic of the most highly purified caveolae/raft fractions, i.e., ACR > NDCR > DRM.

Fluorescence Polarization of Probe Molecules that Preferentially Distribute in "Solid−Gel" or "Fluid−Liquid-Crystalline" Lipid Phases (Parinaric Acids, NBD-Stearic acid, and DiI_{18}). Long (i.e., 18 carbons) straight chain lipidic fluorescence probes such as *trans*-parinaric acid or NBD-stearic acid (*41*), as well as DiI_{18} (*42*), preferentially partition into solid gel phases rather than fluid liquid-crystalline phases in the lateral plane of the lipid bilayer. *cis*-Parinaric acid exhibits no selectivity for either phase.

All the straight acyl chain fatty acid probes (i.e., *trans*-parinaric acid and NBD-stearic acid) detected the same or even less fluorescence polarization in DRM than in NR domains (Table 2). In contrast, fluorescence polarizations of the two straight chain fatty acid probes [i.e., *trans*-parinaric acid and NBD-stearic acid (Table 2)] were significantly lower ($p < 0.05$) in DRM than in NDCR or ACR. For the kinked acyl chain probe, *cis*-parinaric acid (Table 2), the fluorescence polarization pattern in the various membrane fractions was in the following order: ACR > NDCR > DRM > NR ($p < 0.05$). Comparison of the fluorescence polarization of *cis*-parinaric acid and *trans*-parinaric acid (Table 2) showed that in general the fluorescence polarization of *cis*-parinaric acid was lower than that of *trans*-parinaric acid in the same membrane fraction. This was consistent with the fact that *cis*-parinaric acid exhibits equal selectivity for either solid−gel or fluid liquid-crystalline phases. Since the degree of polarization is lower in fluid liquid-crystalline phases, the average polarization of *cis*-parinaric acid was predicted to be lower than that of *trans*-parinaric acid in solid−gel phases. The data supported this prediction.

Table 3: Transbilayer Structure of Caveolae/Raft Domains and Plasma Membranes Determined Using Diphenylhexatriene Probes (DPH, TMA-DPH, DPH-propionic acid)[a]

membrane	polarization
diphenylhexatriene	
DRM	0.2912 ± 0.0036^{b}
nondetergent caveolae/rafts	$0.3032 \pm 0.0028^{b,c}$
affinity-purified caveolae/rafts	$0.3177 \pm 0.0019^{b,c}$
noncaveolae/nonrafts	0.2873 ± 0.0026^{c}
DPH-TMA	
DRM	0.2784 ± 0.0034^{b}
nondetergent caveolae/rafts	0.2688 ± 0.0028^{c}
affinity-purified caveolae/rafts	$0.2711 \pm 0.0024^{b,c}$
noncaveolae/nonrafts	0.2680 ± 0.0061^{c}
DPH-propionic acid	
DRM	0.2844 ± 0.0045^{d}
nondetergent caveolae/rafts	$0.2902 \pm 0.0026^{b-d}$
affinity-purified caveolae/rafts	$0.3011 \pm 0.0028^{b-d}$
noncaveolae/nonrafts	0.2838 ± 0.0017^{d}

[a] DPH, TMA-DPH, and DPH-propionic acid were incorporated at low, non-self-quenching levels into purified PM and caveolae/rafts as described in Materials and Methods. Relative fluorescence polarization values represent the means ± the standard deviation ($n = 7$). [b] $p < 0.05$ vs noncaveolae/nonrafts. [c] $p < 0.05$ vs DRM. [d] $p < 0.05$ vs DPH-TMA.

In summary, qualitative analysis of fluorescence polarization of the straight chain 18-carbon fluorescent fatty acid probes did not detect stronger polarization in DRM versus that in NR domains. While the kinked chain *cis*-parinaric acid detected slightly stronger polarization in DRM versus NR domains, this polarization was still much lower than that in ACR. Thus, in general, the fluorescence polarization of the respective probes was dependent on the type of membrane fraction examined in the following order: ACR (least fluid) > NDCR > DRM ≥ NR (most fluid).

Fluorescence Polarization and Emission Intensity of Diphenylhexatriene (DPH). The above polarization data (Tables 1 and 2) suggested that (i) both gel and liquid-crystalline phases were more rigid in ACR, NDCR, and DRM and/or (ii) the probes sensed an intermediate lipid phase enriched in the various lipid raft preparations as compared to NR. This possibility was further examined through the use of DPH, a probe molecule that preferentially distributes in and detects the "intermediate liquid ordered" lipid phase. Since DPH has no preference for coexisting in gel versus fluid liquid-crystalline phases (*43*), the fluorescence polarization of DPH has been used to show the extent to which acyl chains in caveolae isolated by use of detergents (DRM) are organized in the liquid ordered phase (*44*, *45*). To determine whether this was also true for NDCR and ACR, DPH polarization was assessed not only in DRM but also in NDCR, ACR, and NR. To ensure that DPH itself did not perturb the lipid structures, the various membrane fractions were incubated with DPH at a low ratio of DPH to membrane protein (i.e., 0.1 μg/100 μg) to maximally incorporate the probe as described in Materials and Methods. The data showed that the DPH polarization was lowest in NR but significantly higher in the various lipid raft preparations in the following order: ACR > NDCR > DRM (Table 3). These data were consistent with the presence of a disordered liquid phase in all three lipid raft preparations, especially in the ACR and NDCR, but less so in DRM (Table 3).

Fluorescence Polarization of Probe Molecules that Preferentially Distribute into Outer and Inner Leaflets of the Membrane (DPH-TMA and DPH-Pro). Previous studies with other cell lines show that the DPH polarization is weaker in the outer (exofacial) leaflet than in the inner (cytofacial) leaflet of the PM; this has been interpreted as indicating the outer leaflet acyl chains are more fluid than those of the inner leaflet (reviewed in refs *46*−*48*). Due to its positive charge, DPH-TMA appears to be selectively localized in the outer leaflet which is enriched in positively charged but essentially devoid of negatively charged lipids. The negatively charged DPH-Pro appears to localize in the PM inner leaflet which contains predominantly negatively charged lipids (*47*, *49*).

The fluorescence polarization of the outer leaflet selective probe was lowest in NR [0.2873 ± 0.0026 (Table 3)]. Polarization of DPH-TMA was significantly stroner ($p < 0.050$) in all lipid raft preparations as compared to NR as follows: ACR > NDCR > DRM > NR. Thus, the outer leaflet of ACR appeared to be the least fluid while that of DRM the most fluid.

In contrast to the results described above, DPH-propionic acid polarization was lowest in NR, i.e., 0.2838 ± 0.0017, essentially equivalent to that in DRM, i.e., 0.2844 ± 0.0034 (Table 3). Polarization of DPH-propionic acid was significantly stronger ($p < 0.050$) only in the NDCR and ACR: ACR > NDCR > DRM and NR. Since fluidity is inversely related to polarization, the inner leaflet of the NDCR and ACR appeared to be less fluid than that of DRM and NR.

Comparison of DPH-TMA (outer leaflet probe) and DPH-propionic acid (inner leaflet probe) in each of the membrane fractions suggested the presence of a transbilayer fluidity gradient in each of the various membrane fractions. Qualitatively, the fluorescence polarization values of the DPH-propionic acid probe were higher than those of the DPH-TMA probe in all cases (Table 3), indicating that the outer leaflet is more fluid than the inner leaflet in each respective membrane fraction. However, quantitative analysis showed that the difference in polarization (P), defined as PDPH-propionic acid minus PDPH-TMA, was markedly dependent on the membrane fraction being examined in the following order: ACR ($P = 0.0300$) > NDCR ($P = 0.0214$) > NR ($P = 0.0158$) > DRM ($P = 0.0060$). Thus, DRM exhibited the smallest transbilayer fluidity difference, nearly 2.6-fold smaller than that of NR. In contrast, NDCR and ACR exhibited the highest transbilayer fluidity differences, both of which were greater (1.4- and 1.9-fold, respectively) than that of NR. Thus, among the various lipid raft preparations, NDCR and ACR exhibited the highest transbilayer fluidity differences (3.6- and 5-fold, respectively) as compared to DRM.

These findings were consistent with earlier studies indicating that the PM inner leaflet fluidity is lower than that of the outer leaflet. The data given above demonstrated for the first time that this is the case not only for the entire PM (*46*) but also for the lipid raft versus non-lipid raft domains therein. The transbilayer fluidity difference as compared to that of the NR appeared to be greater for the two membrane fractions not utilizing detergents (i.e., NDCR and ACR). In contrast, the transbilayer fluidity difference in DRM was markedly smaller than that of any other membrane fraction that was examined, including the NR.

Contribution of Detergents to Structure and Fluidity. Because detergents such as Triton X-100 are known to solubilize membranes, the possibility that some of the

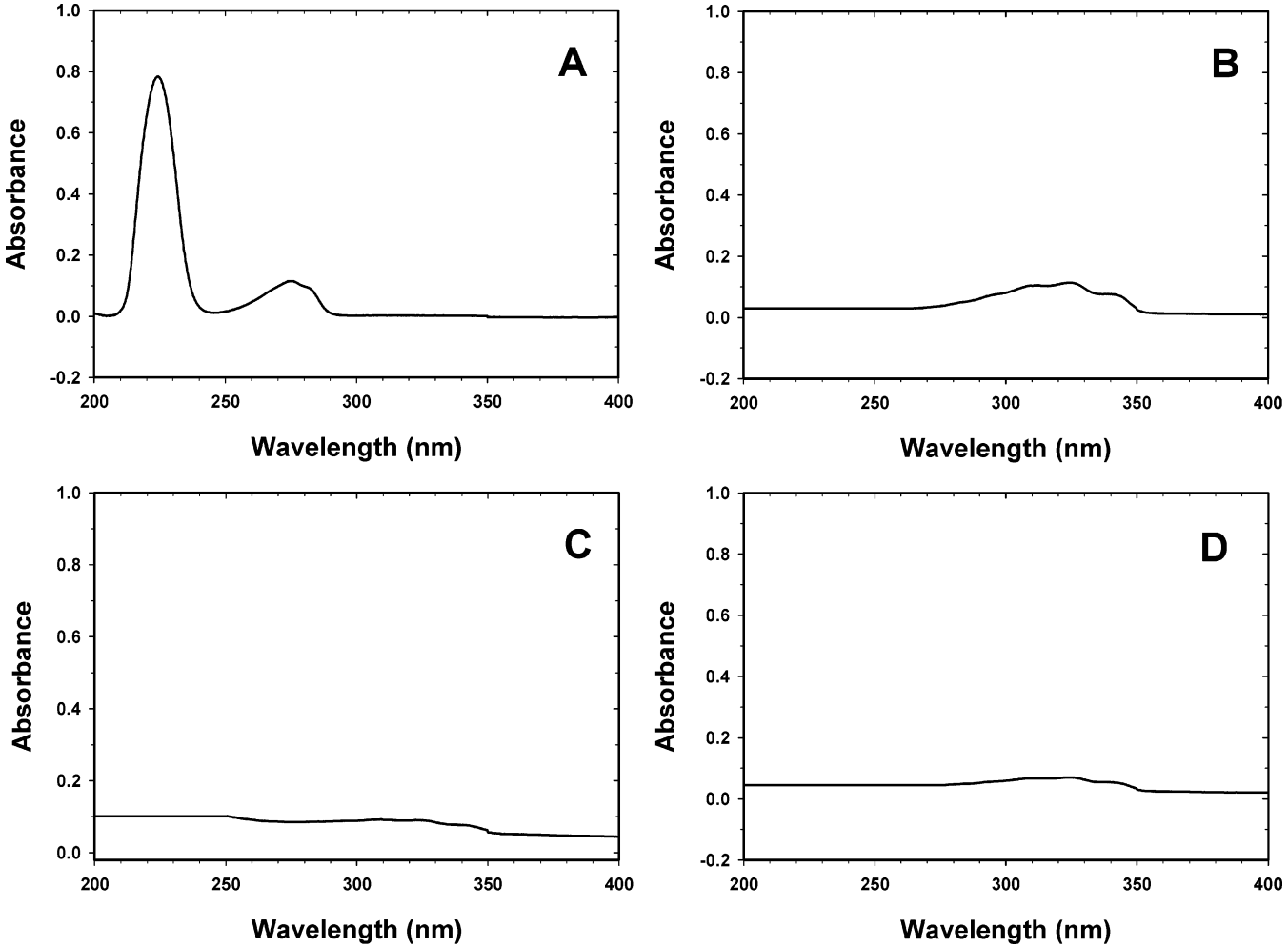

FIGURE 3: Detection of detergent Triton X-100 via absorbance spectra of Triton X-100 and caveolae/raft-enriched membrane fractions: (A) absorbance spectrum of Triton X-100 in PIPES buffer (2 mL, 5% solution), (B) absorbance spectrum of DRM in PIPES buffer (3.5 μg/2 mL), (C) absorbance spectrum of nondetergent caveolae/lipid rafts in PIPES buffer (3.5 μg/2 mL), and (D) absorbance spectrum of affinity-purified caveolae/lipid rafts in PIPES buffer (3.5 μg/mL).

differences in the structural and cholesterol dynamic properties of DRM versus NDCR and ACR might be due to the presence of Triton X-100 in the DRM was considered. To test this hypothesis, the absorbance spectra of all three membrane preparations and Triton X-100 in TNE buffer were obtained (Figure 3). The absorbance spectrum of the detergent Triton X-100 in TNE buffer demonstrated a major peak with a maximum near 224 nm and a minor doublet with maxima near 270 and 280 nm (Figure 3A). The limit of detection of Triton X-100 by this method was 25 nM, determined as described previously (*50*). It is noteworthy that the absorbance spectrum of Triton X-100 in ethanol (not shown) was very similar to that taken in aqueous solvent. The absorbance spectrum of DRM did not reveal any of the peak maxima typical of Triton X-100 (Figure 3B). As expected, the absorbance spectra of the caveolae/lipid raft domains isolated by the detergent-free methods also contained no absorbance peaks typical of Triton X-100: NDCR (Figure 3C) and ACR (Figure 3D). In addition to the method detection limit, another useful parameter in determining that the detergent likely did not influence results is the cell lipid/detergent ratio. A lipid analysis of the MDCK membrane fractions isolated in this work is not currently available and was not performed, since such analysis is outside the scope of this work and would merit its own study. However, when all of the solution concentrations are taken into account, the initial ratio (before isolation of the membranes but after addition of Triton X-100) of detergent to cells is 2.85×10^{-15} mol of detergent/cell. After isolation, the amount of Triton X-100 was too low to detect (Figure 3), indicating most of the detergent was removed during processing and agreeing with previous studies (*44*, *53*, *54*). Thus, the significant differences in the structure and fluidity of DRM versus those of NDCR, ACR, and NR of PM were not due to a high concentration of detergent in the DRM.

Spontaneous and SCP-2-Mediated Sterol Transfer from DRM and DSM. Although the data given above indicate that the structure (crystalline vs monomeric) and fluidity (polarization under non-self-quenching conditions) of DHE in DRM differed significantly from those of NDCR and ACR, nothing is known regarding the effect of these differences on (i) spontaneous sterol transfer from DRM as compared to that in the other caveolae/lipid raft preparations or (ii) the response of DRM versus other caveolae/lipid raft preparations to intracellular sterol carrier protein-2. To begin to resolve these issues, a previously established fluorescent DHE exchange assay was utilized as described in Materials and Methods.

The initial polarization of DHE in the donor DRM was 0.1153 ± 0.0016, consistent with self-quenching due to the

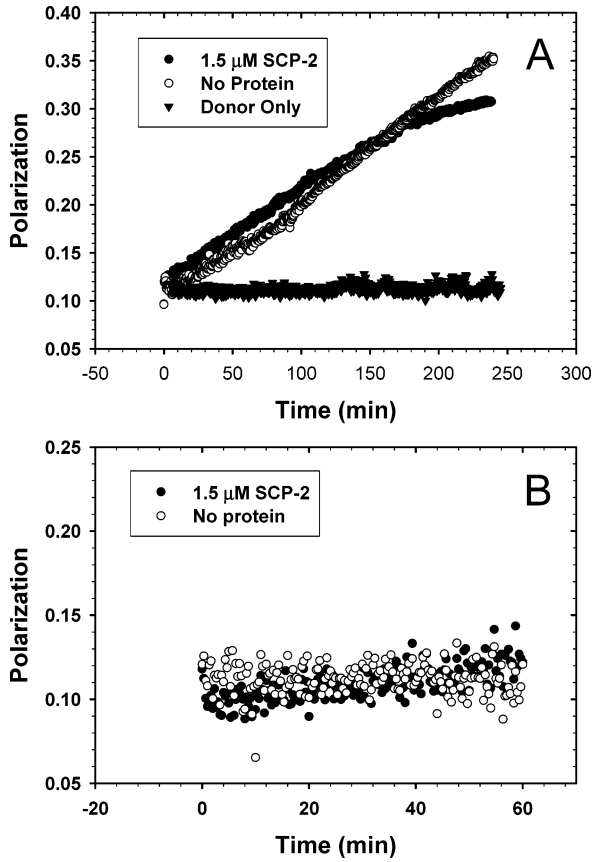

FIGURE 4: Sterol transfer from detergent-resistant membranes (DRM) and detergent-soluble membranes (DSM). (A) Effect of SCP-2 on sterol exchange between DRM. Dehydroergosterol (DHE) exchange between DRM donors (1.75 μg of protein/mL) and DRM acceptors (17.5 μg/mL) was assessed by monitoring polarization as described in Materials and Methods. White circles show the spontaneous sterol exchange after addition of a 10-fold excess of acceptor DRM. Black circles show the effect of SCP-2 (1.5 μM) on the sterol exchange between donor and acceptor DRM. For comparison, a donor-only polarization curve is shown (▼). (B) Effect of SCP-2 on sterol exchange between DSM. DHE exchange was assessed as described for panel A, except that DSM donor and DSM acceptor membranes were used as described in Materials and Methods. White circlec show the spontaneous sterol transfer from donor DSM after addition of a 10-fold excess of acceptor DSM. Black circles show the effect of 1.5 μM SCP-2 on the sterol exchange between donor DSM and acceptor DSM.

presence of high levels of DHE [Figure 4A (○)]. In the absence of acceptor DRM, DHE polarization in DRM donors did not significantly change over several hours [Figure 4A (▼)]. However, surprisingly, addition of a 10-fold excess of acceptor DRM elicited a fast increase in polarization, consistent with release from self-quenching due to exchange of DHE (donor) and cholesterol (acceptor). From a starting polarization of 0.1146 ± 0.0024, the polarization of DHE exhibited a nearly linear increase and did not saturate until reaching a polarization near 0.45 [Figure 4A (○)]. The initial rate of spontaneous molecular sterol transfer from DRM, calculated as described in Materials and Methods, was 0.387 ± 0.072 pmol/min (Table 4). Since the spontaneous exchange was approximately linear over the entire time period that was examined, the exchangeable fraction (f_1) for spontaneous sterol exchange was set to unity (Table 4).

To determine if sterol transfer from DRM was responsive to a sterol transfer protein, i.e., sterol carrier protein-2 (SCP-2), the sterol exchange was monitored in the presence of SCP-2 as described in Materials and Methods. SCP-2 is a protein present in all mammalian tissues examined to date, which enhances sterol transfer between a majority of membranes, with erythrocytes being a rare exception (*51*). Therefore, SCP-2 was used to probe sterol dynamics of DRM and DSM. Addition of SCP-2 to donor alone failed to significantly alter DHE polarization (not shown), consistent with earlier studies of model and biological membranes (reviewed in ref *40*). The SCP-2-mediated exchange of sterol between DRM donors (DHE-containing) and DRM acceptors resulted in release from self-quenching and increased DHE fluorescence polarization [Figure 4A (●)]. The shape of the 4 h SCP-2-mediated sterol exchange curve was consistent with a more rapid and saturable process as compared to the spontaneous exchange between DRM which was still linear over this time period. The SCP-2-mediated exchange curve reached a maximal polarization of 0.3382 ± 0.0042 by 4 h, while the spontaneous exchange was still linear (polarization near 0.3600) at 4 h, suggesting SCP-2 acted to enhance sterol transfer at early time points but slightly inhibited sterol exchange at later time points. The initial rate of SCP-2-mediated sterol transfer (0.619 ± 0.037 pmol/min) was 1.6-fold faster than that of spontaneous sterol transfer from DRM (Table 4). Since kinetic analysis of the SCP-2-mediated sterol exchange was unable to resolve more than one exchangeable domain, the exchangeable fraction (f_1) for each exchange was set to unity (Table 4).

In contrast to that of DRM, the spontaneous sterol exchange curve for DSM was essentially unchanged over the 4 h time period that was examined [Figure 4B (○)]. The initial polarization of DHE near 0.1163 ± 0.0034 was essentially unaltered during spontaneous exchange between donor DSM (containing DHE) and acceptor DSM over the 4 h incubation [Figure 4B (○)]. The initial rate of spontaneous sterol transfer from DSM was calculated to be 0.024 ± 0.009 pmol/min, 14-fold slower than the rate of spontaneous sterol transfer from DRM (Table 4). SCP-2 elicited a slight change in fluorescence polarization, but the resulting polarization curve did not have a steep slope [Figure 4B (●)], in contrast to that observed with SCP-2 and DRM [Figure 4A (●)]. The initial rate of SCP-2-mediated sterol transfer from DSM was 0.087 ± 0.041 pmol/min, 3.6-fold faster than the rate of spontaneous sterol transfer from DSM but still nearly 4-fold slower than the rate of SCP-2-mediated sterol transfer from DRM (Table 4). Kinetic analysis of the spontaneous sterol exchange between DSM as described in Materials and Methods resolved a long half-time ($t_{1/2}$ = 755 ± 55 min) and an exchangeable fraction (f_1 = 0.229 ± 0.021) (Table 4). For the SCP-2-mediated sterol exchange from DSM, kinetic analysis resolved a 2-fold faster $t_{1/2}$ (382 ± 34 min) but an essentially unaltered exchangeable fraction f_1 (0.251 ± 0.028).

In summary, spontaneous sterol transfer from DRM, but not DSM, was rapid and essentially not saturable during the 4 h time period of the exchange. Because spontaneous sterol transfer from DRM was so rapid, SCP-2 elicited only a modest increase in the rate of sterol transfer. In contrast, spontaneous sterol transfer from DSM was comparatively slow and relatively unresponsive to SCP-2. As discussed above, these properties of DRM (Figure 3B) and DSM (not shown) were not due to contamination with residual Triton X-100. If one assumed that DRM are enriched in caveolae/

Table 4: Initial Rates and Kinetic Multiexponential Analysis of Molecular Sterol Exchange Determined by the Effect of Sterol Carrier Protein-2[a]

	protein added	initial rate (pmol/min)	$t_{1/2}$ (min)	f_1	f_2
DRM	none	0.387 ± 0.072[b]	–	1.000	–
	SCP-2	0.619 ± 0.037[b,c]	–	1.000	–
DSM	none	0.024 ± 0.009	755 ± 55	0.229 ± 0.021	0.771 ± 0.034
	SCP-2	0.087 ± 0.041	382 ± 34[c]	0.251 ± 0.028	0.749 ± 0.028
nondetergent caveolae/rafts	none	0.127 ± 0.037	194 ± 24	0.421 ± 0.021	0.579 ± 0.004
	SCP-2	0.163 ± 0.025	131 ± 17[c]	0.520 ± 0.027[c]	0.480 ± 0.041
affinity-purified caveolae/rafts	none	0.105 ± 0.028	172 ± 15	0.472 ± 0.033	0.528 ± 0.029
	SCP-2	0.234 ± 0.021[b,c]	121 ± 26[c]	0.583 ± 0.022[b,c]	0.417 ± 0.031
noncaveolae/nonrafts	none	0.024 ± 0.009	412 ± 32	0.371 ± 0.041	0.629 ± 0.025
	SCP-2	0.032 ± 0.005	384 ± 47	0.401 ± 0.031	0.599 ± 0.032

[a] Fluorescence polarization exchange curves for the sterol transfer from caveolae/raft donors to caveolae/raft acceptors were measured in the absence or presence of SCP-2 (1.5 μM) followed by determination of initial rates and kinetic analysis as described in Materials and Methods. Unless otherwise stated, half-times ($t_{1/2}$) were in minutes, while f_1 and f_2 represent the fractions due to the exchangeable and nonexchangeable components, respectively. Values represent the means $\pm$ the standard deviation ($n = 3-4$). [b] $p < 0.05$ vs nondetergent caveolae/raft. [c] $p < 0.05$ vs no protein added.

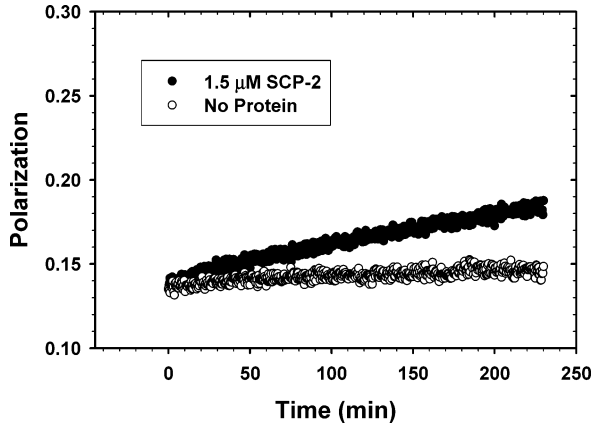

FIGURE 5: Sterol transfer from nondetergent caveolae/rafts. Dehydroergosterol (DHE) exchange between nondetergent caveolae/raft donor (1.75 μg of protein/mL) and nondetergent caveolae/raft acceptor (17.5 μg of protein/mL) was assessed by monitoring DHE polarization as described in Materials and Methods. White circles show the spontaneous sterol exchange between donor nondetergent caveolae/rafts after addition of a 10-fold excess of acceptor nondetergent caveolae/rafts. Black circles show the effect of 1.5 μM SCP-2 on the sterol exchange between donor and acceptor nondetergent caveolae/rafts.

lipid rafts, as indicated by the Western blots (Figure 1), while DSM are enriched in nonrafts, these data suggest that spontaneous sterol transfer from lipid rafts may be rapid while that from nonrafts is very slow in comparison.

Spontaneous and SCP-2-Mediated Sterol Transfer from NDCR. To determine if the high spontaneous rate of sterol transfer from DRM was a unique property of this lipid raft-enriched fraction, the experiments described above were repeated with NDCR isolated as described in Materials and Methods. Since the NDCR isolation method did not produce a comparable DSM fraction, it was not possible to directly obtain the sterol exchange dynamics from this membrane domain. The initial polarization of DHE in donor NDCR was near 0.14 (Figure 5), consistent with self-quenching of the DHE therein. In the absence of acceptor NDCR, DHE polarization was not altered over the 4 h time frame of exchange (not shown). In contrast, in the presence of acceptor NDCR, slow spontaneous sterol transfer was detectable as an increase in DHE polarization [Figure 5 (○)]. The initial rate of spontaneous molecular sterol transfer from NDCR was 0.127 ± 0.037 pmol/min, nearly 3-fold slower than that exhibited by DRM (Table 4). Kinetic analysis resolved a half-time of spontaneous sterol transfer for the NDCR of $\sim 194 \pm 24$ min (Table 4) and an exchangeable fraction f_1 of 0.421 ± 0.021, which was 2.4-fold smaller than that for DRM (Table 4).

Sterol transfer from NDCR was more responsive to sterol carrier protein SCP-2. When SCP-2 was added to NCDR donors alone, a change in DHE fluorescent polarization was observed (not shown). However, when SCP-2 was added to NCDR donors with a 10-fold excess of acceptor membranes, there was a more rapid and extensive increase in DHE polarization [Figure 5 (●)]. These results indicated that SCP-2 enhanced sterol transfer from the NCDR membranes. The initial rate of SCP-2-mediated sterol exchange between NDCR was 0.163 ± 0.025 pmol/min, 1.3-fold faster than that of spontaneous sterol exchange from NDCR (Table 4). Kinetic analysis of SCP-2-mediated sterol transfer curves from NDCR indicated that SCP-2 decreased the $t_{1/2}$ of the exchangeable sterol pool by 32% from 194 ± 24 to 131 ± 17 ($p < 0.05$) and increased the size of the exchangeable sterol pool by 1.23-fold from 0.421 ± 0.021 to 0.520 ± 0.027 ($p < 0.05$) (Table 4).

In summary, the spontaneous molecular transfer of sterol from NDCR was significantly slower (i.e., nearly 3-fold) than that exhibited by DRM. Furthermore, SCP-2 increased the rate of sterol transfer from NDCR, but the initial rate of SCP-2-mediated sterol transfer from NDCR was still 3.8-fold slower than that mediated by SCP-2 in DRM. Thus, both the spontaneous and SCP-2-mediated sterol dynamics of NDCR differed markedly from those of DRM.

Spontaneous and SCP-2-Mediated Sterol Transfer from ACR. Concanavalin A−Sepharose binding affinity chromatography was used to simultaneously fractionate ACR, the adherent fraction, and NR, the nonadherent fraction (equivalent to DSM), from purified PM vesicles isolated from MDCK cells as described in Materials and Methods. Spontaneous sterol transfer from ACR was slower than that exhibited by DRM. Consistent with DHE self-quenching, the initial fluorescence polarization of DHE in donor ACR was 0.1327 ± 0.0046 [Figure 6A (○)]. In the absence of acceptor, ACR was unaltered over the 4 h time frame of exchange (not shown). Upon addition of a 10-fold excess of acceptor ACR, DHE spontaneously transferred from the donor to acceptor membranes as indicated by increased polarization

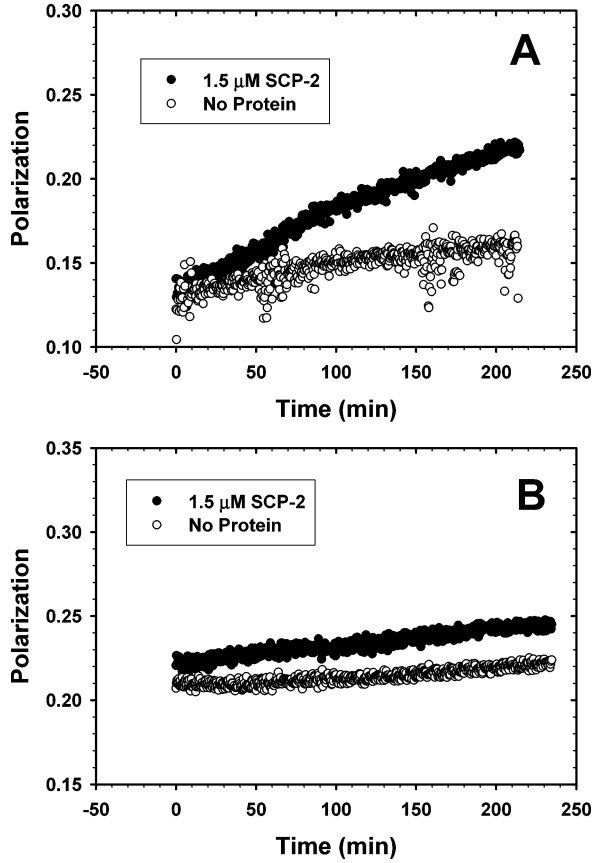

FIGURE 6: Sterol transfer from affinity-purified caveolae/rafts. (A) Effect of SCP-2 on sterol exchange between affinity-purified caveolae/rafts. Dehydroergosterol (DHE) exchange between affinity-purified caveolae/raft donors (1.75 μg of protein/mL) and affinity-purified caveolae/raft acceptors (17.5 μg of protein/mL) was assessed by monitoring DHE polarization as described in Materials and Methods. White circles show the spontaneous sterol exchange between donor and acceptor affinity-purified caveolae/rafts. Black circles show the effect of 1.5 μM SCP-2 on the sterol exchange between donor and acceptor affinity-purified caveolae/rafts. (B) Effect of SCP-2 on sterol transfer from affinity-purified caveolae/raft domains which did not bind the concanavalin A−Sepharose affinity column. DHE exchange was assessed as described for panel A. White circles show the spontaneous sterol transfer from donor caveolae/raft membranes after addition of a 10-fold excess of acceptor caveolae/raft membranes. Black circles show the effect of 1.5 μM SCP-2 on the sterol transfer from donor caveolae/raft membranes to a 10-fold excess of acceptor caveolae/raft membranes.

[Figure 6A (○)]. The initial rate of spontaneous molecular sterol transfer from ACR was 0.105 ± 0.028 pmol/min, 3.7-fold slower than that from DRM (Table 4). Kinetic analysis as described in Materials and Methods showed that the exchange curves for spontaneous molecular sterol transfer from ACR best fit two components: an exchangeable sterol pool with a $t_{1/2}$ of 172 ± 15 min and a fraction f_1 of 0.472 ± 0.033 of total sterol, which was 2.1-fold smaller than that exhibited by DRM (Table 4). In addition, ACR domains contained a very slow ($t_{1/2}$ of days), essentially nonexchangeable sterol pool representing 0.528 ± 0.029 of the total ACR domain sterol (Table 4). The size of the nonexchangeable sterol pool was similar to that observed in NDCR, which did not contain a detectable nonexchangeable pool, but significantly different from the sterol organization of DRM. When sterol transfer from donor to acceptor ACR domains was probed with SCP-2, the DHE polarization increased markedly [Figure 6A (●)]. SCP-2 enhanced the initial rate of molecular sterol transfer from ACR essentially 2-fold from 0.105 ± 0.028 to 0.234 ± 0.021 pmol/min ($p < 0.05$) (Table 4). Kinetic analysis of the SCP-2-mediated sterol exchange curves showed that SCP-2 enhanced the sterol transfer from ACR domains by decreasing the $t_{1/2}$ of exchange by nearly 30% from 172 ± 15 to 121 ± 26 min ($p < 0.05$) and by increasing the fraction of exchangeable sterol by 24% from 0.472 ± 0.033 to 0.583 ± 0.022 ($p < 0.05$) (Table 4). Thus, SCP-2 altered the sterol dynamics of ACR domains significantly more than in either DRM or NDCR. In contrast, NR exhibited markedly slower spontaneous sterol transfer [Figure 6B (○)] and lacked responsiveness to SCP-2 [Figure 6B (●)]. The initial rate of molecular DHE transfer from NR was 0.024 ± 0.009 pmol/min, 4.4-fold slower than that from ACR (Table 4). The half-time of spontaneous sterol transfer from NR was slow, 412 ± 32 min, which was 2.4-fold slower than that from ACR (Table 4). The fractional contribution of exchangeable sterol domain in NR was 0.371 ± 0.041, which was 22% smaller than that exhibited by ACR (Table 4). SCP-2 did not significantly alter any of the parameters of sterol dynamics in NR, indicating NR contained both exchangeable and nonexchangeable sterol domains.

In summary, although ACR exhibited the slowest initial rate of spontaneous sterol transfer of any of the examined lipid raft-enriched membrane fractions, it was still more than 4-fold faster than the rate of spontaneous sterol transfer from NR. The NR had the largest fraction of nonexchangeable sterol domain and was unresponsive to SCP-2.

DISCUSSION

There has been a paucity of information regarding the structural organization of cholesterol, fluidity, transbilayer structure, and cholesterol dynamics of caveolae/raft domains (reviewed in ref *3*). Further, there has been an ongoing debate about what constitutes a lipid raft/caveolae (reviewed in refs *17* and *18*). These studies also indicate the use of detergents can alter the nature and/or composition of the resultant isolated rafts. To begin to address these issues, this study utilized three distinct methods to obtain caveolae/rafts from MDCK cells: (i) a Triton X-100-based method for producing detergent-resistant membranes (DRM) and detergent-soluble membranes (DSM), (ii) a nondetergent isolation based on the Percoll and OptiPrep gradients which first isolates PM and then fractionates caveolae/lipid rafts according to density (*21*), and (iii) an affinity chromatography-based method wherein PM are first isolated by sucrose density fractionation and then separated into affinity-purified caveolae/lipid rafts (ACR) and noncaveolae/nonrafts (NR) by use of concanavalin A−Sepharose affinity chromatography (*1*, *18*, *25*). Note that these techniques do not distinguish caveolar lipid rafts from noncaveolar lipid rafts. The data presented herein demonstrate for the first time that the function (cholesterol exchange dynamics) and structure (lipid fluidity) of DRM share qualitative, but not quantitative, properties exhibited by caveolae/lipid rafts isolated from MDCK cells by nondetergent methods in the following order: DRM < nondetergent caveolae/rafts (NDCR) < ACR. The key findings of this study are enumerated below.

First, it was shown for the first time that the structural form of sterol (monomeric vs crystalline) in DRM differed markedly from that of all other examined MDCK PM

fractions. DRM, but not NDCR or ACR, contained a significant amount of crystalline sterol (i.e., near 10%). This was unexpected as previous compositional analyses of isolated PM and multiphoton images of sterol in the PM of living cells detected very little crystalline sterol, generally near 1% (*4*). In contrast, crystalline sterol is associated primarily with lysosomes (*4*, *52*). These data suggest that significant amounts of crystalline sterol in DRM arise during the preparation. Since DRM are isolated from whole cells, the crystalline sterol in DRM may arise in part by selective retention of cholesterol from lysosomes. Alternatively, as the detergents used in DRM isolation selectively extract certain phospholipids, the resulting high sterol/phospholipid ratio (reviewed in refs *37* and *38*) could lead to phase separation of sterol into the crystalline form. The sterol phase has been shown to separate into crystalline sterol at a high cholesterol/phospholipid molar ratio in model membranes (reviewed in ref *4*).

Second, the sterol fluidity in DRM differed markedly from that of the other MDCK PM fractions using DHE. Although synthetic sterol probe molecules may have deleterious effects on membrane structure and function, such as NBD-cholesterol, sterol-phenol, or nitroxide-cholesterol, to our knowledge there are no data demonstrating toxic or adverse effects of DHE added to cultured cells or fed to animals (reviewed in refs *6*−*9*). DHE is a natural component of membranes in other eukaryotic organisms, including yeast and sponges (reviewed in refs *6* and *10*−*12*). When DHE is simply fed to cultured cells (*4*, *10*, *13*) or animals (*14*, *15*), it is readily incorporated into membranes or lipoproteins in the absence of additional chemicals, catalysts, or experimental manipulations. Incorporation of DHE to up to 80−90% of total membrane sterol has no adverse effects on the sterol/phospholipid ratio, fatty acid composition, sterol distribution, or receptor−effector interactions sensitive to sterols or sterol structure (*10*, *16*).

The fluorescence polarization of DHE in DRM was higher than that of NDCR. Consistent with this observation, electron spin resonance studies comparing spin-labeled cholestane mobility in model membranes with that in DRM isolated from RBL-2H3 cells also conclude there is a less fluid sterol environment in the DRM (*20*). However, quantitative analyses indicated that the fluorescence polarization of DHE in DRM was the highest of any of the lipid raft-enriched PM fractions that were examined: DRM > NDCR > ACR. Since fluorescence polarization provides a relative measure of the mobility and fluidity of the probe, these data suggest that the sterol in DRM was significantly less mobile than that in the NR fraction but more mobile than that in any of the other lipid raft-enriched fractions of the PM as follows: NR > DRM > NDCR > ACR. The physical basis for the uniquely lower fluidity of sterol in DRM and other caveolae/lipid raft preparations was not clear, but several possibilities may be considered. (i) Contaminating detergent may increase the fluidity of sterol in DRM as compared to other caveolae/lipid raft preparations. However, the data showed that DRM had the lowest fluidity and did not contain detectable amounts of Triton X-100; therefore, our data were consistent with earlier studies which also demonstrated the absence of detergent in DRM (reviewed in ref *53*). (ii) Crystalline sterol in DRM may contribute to the higher fluidity and mobility of sterol in DRM. (iii) Sterol may partition into a liquid ordered phase in DRM, NDCR, and ACR. Consistent with the latter possibility, electron spin resonance of spin-labeled cholestane in model membranes and DRM isolated from RBL-2H3 cells suggested that the sterol partitioned into a liquid ordered phase in DRM (*20*). Given that similar results were obtained with the naturally occurring fluorescent sterol DHE and the spin-labeled sterol cholestane, the same type of sterol environment (liquid ordered phase) exists with the lowest degree of order in DRM, intermediate in NDCR, and highest in ACR. These data implied that the physical state of the liquid ordered phase in DRM is unique or that the relative amount of liquid ordered phase in lipid raft-enriched PM fractions is highly dependent on the method used for isolation.

Third, as compared to that of NR, the fluidity of lipid acyl chains detected by fluorescence polarization of lipidic probes in NDCR and ACR (but not DRM) was lower, consistent with a liquid disordered state. In general, the polarizations of DiI_{18} and *cis*-parinaric acid (but not DPH, *trans*-parinaric acid, or NBD-stearic acid) appeared to be significantly higher in DRM than in NR. In contrast, the fluorescence polarizations of all five lipidic probes were higher in NDCRs and ACR than in NR. Model membrane studies show that DPH polarization in the non-fluid gel phase and in the liquid crystalline phase is 0.381 and 0.095, respectively, while that in the liquid disordered phase is intermediate (*54*). As shown herein, the fluorescence polarization of DPH in ACR was 0.3177 ± 0.0019 (Table 3), well within the range of DPH in the liquid ordered phase of model membranes (*54*). With regard to the other lipid raft preparations, DPH polarization in NDCR was also higher but not as high as in ACR as in NR, consistent with the presence of a liquid disordered phase. The average DPH polarization in DRM was slightly higher than in NR but did not achieve statistical significance. This was in contrast to earlier fluorescence and electron spin resonance studies of DRM from model membranes and other cell types, suggesting a liquid disordered phase therein (*20*, *54*). Taken together, the acyl chain environment of a variety of non-sterol lipidic fluorophores suggested that (i) the liquid ordered phase is more prevalent in ACR than in NDCR and than in DRM or (ii) the degree of order in equivalent concentrations of liquid ordered phase is higher in ACR than in NDCR and than in DRM.

Fourth, the fluorescence polarizations of the leaflet selective DPH-TMA (exofacial leaflet) and DPH-Pro (cytofacial leaflet) fluorophores were used to examine the relative fluidity of the outer and inner leaflets of lipid raft membranes. Mammalian cell membranes contain transport proteins (phospholipid flippases and translocases) that actively transport negatively charged phospholipids to the cytofacial leaflet (reviewed in ref *49*). Consequently, phosphatidylserine and phosphatidylinositol are on the cytofacial leaflet, while other phospholipids remain in the outer leaflet. Just like the other negatively charged phospholipids, the negatively charged DPH-Pro is expected to be found on the cytofacial leaflet. Hence, DPH-TMA (zwitterionic or non-negative) is expected to be found on the outer leaflet just like other zwitterionic phospholipids, non-negative (phosphatidylcholine and sphingomyelin) phospholipids. The difference in DPH-TMA polarization and DPH-Pro polarization is a measure of the transbilayer fluidity gradient between the two membrane leaflets (reviewed in refs *46*−*48*).

Although in all membrane fractions that were examined the exofacial leaflet appeared to be more fluid, the fluidity gradient was markedly dependent on the membrane fraction being examined with DRM being the smallest: DRM ($P = 0.0060$) < NR ($P = 0.0158$) < NDCR ($P = 0.0214$) < ACR ($P = 0.0300$). Thus, the DRM were unique in exhibiting a 2.6-fold smaller transbilayer fluidity gradient compared to that of NR. In contrast, NDCR and ACR exhibited the highest transbilayer fluidity differences, 1.4- and 1.9-fold greater, respectively, than that of NR. While the exact basis for the DRM exhibiting such a small transbilayer fluidity difference (even lower than in NR) is not known, there are three possible causes. (i) Detergents are known to selectively extract certain phospholipids species (*53*). (ii) DRM may be comprised of a mixture of right-side-out and inside-out orientations (*55*). (iii) Since DRM are isolated from whole cells, they may be composed not only of PM constituents but also of other intracellular membrane components that contain significant amounts of cholesterol (e.g., lysosomes and ER). In contrast, a previous study showed that concanavalin A−Sepharose affinity-purified membranes were oriented right-side-out (*56*). It is important to note that transbilayer fluidity gradients function in modulating the activity of transbilayer-coupled receptors and transporters in the PM (reviewed in ref *57*). Further, the transbilayer gradient is responsive to dietary unsaturated fatty acids, oxidized lipid, anesthetics, and a variety of pathologies (reviewed in refs *46* and *56*). Taken together, the data presented herein indicated that the transbilayer fluidity gradient in lipid raft-enriched membrane fractions was more clearly defined and greater in ACR and NDCR than NR, while that in DRM is actually smaller than in the other PM-enriched fractions.

Fifth, it was shown for the first time that spontaneous sterol transfer from NR and DSM was slow and essentially unresponsive to SCP-2. These findings supported current studies with intact cells indicating that sterol transfer is mediated through proteins localized in the PM (i.e., SRB 1, P-glycoprotein, and ABC-A1) and within the cell (i.e., SCP-2 and caveolin-1) (reviewed in refs *2*, *3*, and *58*).

Sixth, both spontaneous and SCP-2-mediated sterol transfer from lipid raft-enriched PM fractions were highly dependent on the type of preparation used. Although spontaneous sterol transfer from DRM was very rapid (polarizations approached the theoretical limit), SCP-2 did not enhance the already very rapid sterol transfer from DRM. Since SCP-2 did not enhance sterol transfer from DRM, much less DSM and NR, these data do not account for the significant SCP-2-mediated enhancement of sterol transfer from isolated PM vesicles noted earlier (*39*). In contrast to these observations with DRM, spontaneous sterol transfer from NDCR and ACR was moderately faster than from DSM and NR and highly responsive to SCP-2. SCP-2 enhanced the initial rate, decreased the half-time, and increased the size of the exchangeable sterol domain in NDCR and ACR, but not DRM or NR. Notably, the slow spontaneous sterol transfer from all PM fractions (except DRM) was not due to slow transbilayer sterol migration. Transmembrane cholesterol flip-flop across both model membranes and PM (*7*, *59*, *60*) is fast (minutes). Intact cells have evolved very rapid (1−2 min) protein-mediated (i.e., SCP-2 and caveolin-1) and somewhat slower (10−20 min) vesicular intracellular cholesterol trafficking pathways to and from the PM (*1*, *61*). An example of the potential importance of cholesterol transfer by sterol-binding proteins is the movement of sterols from hepatocyte basolateral PM to the bile canilicular region, which occurs by nonvesicular pathways (*62*). Identifying these pathways, the PM domains involved, and protein mediators may provide valuable insight into the function of caveolae/rafts in sterol trafficking. Taken together, these data on spontaneous and SCP-2-mediated sterol dynamics from lipid raft-enriched fractions isolated without the use of detergents (i.e., NDCR and even more so ACR) versus sterol dynamics from NR more closely resembled sterol dynamics from the PM of intact cells than DRM.

Despite the recognition that PM are comprised of multiple types of domains, i.e., rafts versus nonrafts, little is known regarding the fluidity, transbilayer structure, and sterol dynamics of these functionally distinct domains. Although most studies have focused largely on DRM, recent reports in the literature have questioned the purity of lipid rafts prepared from whole cells by use of detergents (*19*) and have postulated that DRM may not necessarily be equivalent to caveolae/lipid rafts in cells or may represent a different fraction of caveolae/lipid rafts than those isolated by methods not using detergents (reviewed in refs *3*, *17*, *18*, *38*, and *55*). Therefore, the investigation presented here was undertaken to isolate both nonraft and raft types of domains from MDCK PM using two classical techniques (DRM and NDCR) and a newly developed method that simultaneously resolves ACR and NR without the use of detergents. These data showed that DRM, NDCR, and ACR qualitatively share several (but not all) structural properties but differ functionally. For example, ACR had no crystalline sterol, were the least fluid, had the highest transbilayer fluidity gradient, and exhibited the most liquid ordered phase. NDCR also had no crystalline sterol but were intermediate in the other properties. In contrast, DRM contained significant amounts of crystalline sterol, were the most fluid, had the smallest transbilayer fluidity gradients, had the largest amount of liquid ordered phase, and most closely resembled NR. Functionally, spontaneous and SCP-2-mediated sterol dynamics of ACR and NDCR were most like those reported for PM and intact cells (*62*). Again, NDCR were intermediate in these properties, while DRM appeared to be anomalous. Although an exhaustive panel of markers was not examined, on the basis of the representative markers that were used, the DRM appeared the least pure while the ACR appeared the most pure of the three lipid raft preparations. In contrast to ACR and NDCR, DRM exhibited significant contamination from both intracellular membrane fractions (e.g., ER). Consistent with these data showing the presence of NR proteins in DRM, a recent proteomics/mass spectrometry approach identified nearly one-third of DRM proteins as being nonspecific contaminants (*19*). These data suggest that the structure and sterol dynamics of DRM are at least in part a product of the detergent isolation procedure or that DRM comprise a distinct lipid raft domain significantly different from those obtained without the use of detergents. Although it would be difficult to claim that any raft preparation is identical to that of lipid rafts in the PM of intact cells, the nondetergent, ACR protocol described herein yielded raft membrane fractions that contained the fewest intracellular organelle contaminants based on select intracellular markers, demonstrated cholesterol exchange dynamics similar to that of intact cells

(reviewed in refs *3* and *63*), and lacked crystalline sterols (*4*), which are absent in intact, viable cells (*4*). Whether these findings can be extended to other cell types remains to be shown.

It is known that the endocytic pathway may involve cholesterol- and sphingolipid-rich domains; however, to date, there is no direct evidence that lipid rafts actually exist in intracellular membranes (*53*). Regardless, it has been suggested that rafts contribute to endocytosis and secretion. This introduces a number of possibilities as enumerated in the review by Brown and London (*53*). The transport of de novo synthesized cholesterol from the ER to the PM is another function attributed to raft microdomains (*45*). The efficiency of cholesterol transport with different raft preparations was not examined in this study nor was endocytosis or secretion. However, we predict the different states (i.e., crystalline, liquid ordered, etc.) of the membranes isolated by different techniques would influence each of these processes and perhaps alter the final destination of the material being transported. Additional studies are needed to evaluate this hypothesis.

In summary, there are many types of preparations for lipid rafts, each with proven value that has provided insights into multiple fields of study. Data obtained with different preparations may reflect not only the purity of the lipid raft isolate but also different populations of lipid rafts isolated from different cells. These results indicate that the methodology selected for raft/caveolae isolation should be carefully considered. Further, care should be taken when interpreting results from DRM and other methods of raft/caveolae isolation.

REFERENCES

1. Frolov, A., Petrescu, A., Atshaves, B. P., So, P. T. C., Gratton, E., Serrero, G., and Schroeder, F. (2000) High density lipoprotein mediated cholesterol uptake and targeting to lipid droplets in intact L-cell fibroblasts, *J. Biol. Chem. 275*, 12769−12780.
2. Smart, E. J. (2005) Caveolae and the regulation of cellular cholesterol homeostasis, in *Advances in Molecular and Cell Biology* (Lisanti, M. P., and Frank, P. G., Eds.) pp 35, Elsevier, Amsterdam.
3. Schroeder, F., Atshaves, B. P., Gallegos, A. M., McIntosh, A. L., Liu, J. C., Kier, A. B., Huang, H., and Ball, J. M. (2005) Lipid rafts and caveolae organization, in *Advances in Molecular and Cell Biology* (Frank, P. G., and Lisanti, M. P., Eds.) pp 3−36, Elsevier, Amsterdam.
4. McIntosh, A., Gallegos, A., Atshaves, B. P., Storey, S., Kannoju, D., and Schroeder, F. (2003) Fluorescence and multiphoton imaging resolve unique structural forms of sterol in membranes of living cells, *J. Biol. Chem. 278*, 6384−6403.
5. Zhang, W., McIntosh, A., Xu, H., Wu, D., Gruninger, T., Atshaves, B. P., Liu, J. C. S., and Schroeder, F. (2005) Structural analysis of sterol distribution in the plasma membrane of living cells, *Biochemistry 44*, 2864−2984.
6. Schroeder, F. (1984) Fluorescent sterols: Probe molecules of membrane structure and function, *Prog. Lipid Res. 23*, 97−113.
7. Schroeder, F., and Nemecz, G. (1990) Transmembrane Cholesterol Distribution, in *Advances in Cholesterol Research* (Esfahami, M., and Swaney, J., Eds.) pp 47−87, Telford Press, Caldwell, NJ.
8. Schroeder, F., Jefferson, J. R., Kier, A. B., Knittell, J., Scallen, T. J., Wood, W. G., and Hapala, I. (1991) Membrane cholesterol dynamics: Cholesterol domains and kinetic pools, *Proc. Soc. Exp. Biol. Med. 196*, 235−252.
9. Schroeder, F., Frolov, A. A., Murphy, E. J., Atshaves, B. P., Jefferson, J. R., Pu, L., Wood, W. G., Foxworth, W. B., and Kier, A. B. (1996) Recent advances in membrane cholesterol domain dynamics and intracellular cholesterol trafficking, *Proc. Soc. Exp. Biol. Med. 213*, 150−177.
10. Hale, J. E., and Schroeder, F. (1982) Asymmetric transbilayer distribution of sterol across plasma membranes determined by fluorescence quenching of dehydroergosterol, *Eur. J. Biochem. 122*, 649−661.
11. Delseth, C., Kashman, Y., and Djerassi, C. (1979) Ergosta-5,7,9-(11),22-tetraen-3β-ol and its 24ϵ-ethyl homolog, two new marine sterols from the red sea sponge *Biemna fortis*, *Helv. Chim. Acta 62*, 2037−2045.
12. Sica, D., Boniforti, L., and DiGiacomo, G. (1982) Sterols of *Candida tropicalis* grown on n-alkanes, *Phytochemistry 21*, 234−236.
13. Schroeder, F., Gallegos, A. M., Atshaves, B. P., Storey, S. M., McIntosh, A., Petrescu, A. D., Huang, H., Starodub, O., Chao, H., Yang, H., Frolov, A., and Kier, A. B. (2001) Recent advances in membrane cholesterol microdomains: Rafts, caveolae, and intracellular cholesterol trafficking, *Exp. Biol. Med. 226*, 873−890.
14. Bergeron, R. J., and Scott, J. (1982) Fluorescent lipoprotein probe, *Anal. Biochem. 119*, 128−134.
15. Bergeron, R. J., and Scott, J. (1982) Cholestatriene and ergostatetraene as in vivo and in vitro membrane and lipoprotein probes, *J. Lipid Res. 23*, 391−404.
16. Gimpl, G., and Fahrenholz, F. (2000) Human oxytocin receptors in cholesterol-rich vs. cholesterol-poor microdomains of the plasma membrane, *Eur. J. Biochem. 267*, 2483−2497.
17. Skwarek, M. (2004) Recent controversy surrounding lipid rafts, *Arch. Immunol. Ther. Exp. 52*, 427−431.
18. Schnitzer, E., Lichtenberg, D., and Kozlov, M. M. (2003) Temperature dependence of the solubilization of dipalmitoylphosphatidylcholine (DPPC) by the non-ionic surfactant Triton X-100, kinetic and structural aspects, *Chem. Phys. Lipids 126*, 55−76.
19. Foster, L. J., de Hoog, C. L., and Mann, M. (2003) Unbiased quantitative proteomics of lipid rafts reveals high specificity for signaling factors, *Proc. Natl. Acad. Sci. U.S.A. 100*, 5813−5818.
20. Ge, M., Field, K. A., Aneja, R., Holowka, D., Baird, B., and Freed, J. H. (1999) Electron spin resonance characterization of liquid ordered phase of detergent resistant membranes from RBL-2H3 cells, *Biophys. J. 77*, 925−933.
21. Smart, E. J., Ying, Y., Mineo, C., and Anderson, R. G. W. (1995) A detergent-free method for purifying caveolae membrane from tissue culture cells, *Proc. Natl. Acad. Sci. U.S.A. 92*, 10404−10408.
22. Gallegos, A. M., McIntosh, A. L., Atshaves, B. P., and Schroeder, F. (2004) Structure and cholesterol domain dynamics of an enriched caveolae/raft isolate, *Biochem. J. 382*, 451−461.
23. Gaus, K., Gratton, E., Kable, E. P. W., Jones, A. S., Gelissen, I., Kritharides, L., and Jessup, W. (2003) Visualizing lipid structure and raft domains in living cells with two-photon microscopy, *Proc. Natl. Acad. Sci. U.S.A. 100*, 15554−15559.
24. Fischer, R. T., Stephenson, F. A., Shafiee, A., and Schroeder, F. (1985) Structure and dynamic properties of dehydroergosterol, Δ5,7,9(11),22-ergostatetraen-3β-ol, *J. Biol. Phys. 13*, 13−24.
25. Atshaves, B. P., Gallegos, A., McIntosh, A. L., Kier, A. B., and Schroeder, F. (2003) Sterol carrier protein-2 selectively alters lipid composition and cholesterol dynamics of caveolae/lipid raft vs. non-raft domains in L-cell fibroblast plasma membranes, *Biochemistry 42*, 14583−14598.
26. Schoer, J., Gallegos, A., Starodub, O., Petrescu, A., Roths, J. B., Kier, A. B., and Schroeder, F. (2000) Lysosomal membrane cholesterol dynamics: Role of sterol carrier protein-2 gene products, *Biochemistry 39*, 7662−7677.
27. Sapin, C., Colard, O., Delmas, O., Tessier, C., Breton, M., Enouf, V., Chwetzoff, S., Ouanich, J., Cohen, J., Wolf, C., and Trugnan, G. (2002) Rafts promote assembly and atypical targeting of a nonenveloped virus, rotavirus, in Caco-2 cells, *J. Virol. 76*, 4591−4602.
28. Parr, R. D., and Ball, J. M. (2003) New donor vector for generation of histidine-tagged fusion proteins using the Gateway Cloning System, *Plasmid 49*, 179−183.
29. Colles, S. M., Wood, W. G., Myers-Payne, S. C., Igbavboa, U., Avdulov, N. A., Joseph, J., and Schroeder, F. (1995) Structure and Polarity of Mouse Brain Synaptic Plasma Membrane: Effects of Ethanol *in vitro* and *in vivo*, *Biochemistry 34*, 5945−5959.
30. Schroeder, F., Hubbell, T., Colles, S. M., and Wood, W. G. (1995) Expression of liver fatty acid binding protein in L-cells: Plasma membrane response to ethanol, *Arch. Biochem. Biophys. 316*, 343−352.

31. Schroeder, F., Myers-Payne, S. C., Billheimer, J. T., and Wood, W. G. (1995) Probing the ligand binding sites of fatty acid and sterol carrier proteins: Effects of ethanol, *Biochemistry 34*, 11919−11927.
32. Schroeder, F., Morrison, W. J., Gorka, C., and Wood, W. G. (1988) Transbilayer effects of ethanol on fluidity of brain membrane leaflets, *Biochim. Biophys. Acta 946*, 85−94.
33. Sweet, W. D., and Schroeder, F. (1986) Plasma membrane lipid composition modulates action of anesthetics, *Biochim. Biophys. Acta 861*, 53−61.
34. Sweet, W. D., Wood, W. G., and Schroeder, F. (1987) Charged anesthetics selectively alter plasma membrane order, *Biochemistry 26*, 2828−2835.
35. Sweet, W. D., and Schroeder, F. (1986) Charged anaesthetics alter LM-fibroblast plasma-membrane enzymes by selective fluidization of inner or outer membrane leaflets, *Biochem. J. 239*, 301−310.
36. Gallegos, A. M., Atshaves, B. P., Storey, S. M., Starodub, O., Petrescu, A. D., Huang, H., McIntosh, A., Martin, G., Chao, H., Kier, A. B., and Schroeder, F. (2001) Gene structure, intracellular localization, and functional roles of sterol carrier protein-2, *Prog. Lipid Res. 40*, 498−563.
37. Eckert, G. P., Igbavboa, U., Muller, W., and Wood, W. G. (2003) Lipid rafts of purified mouse brain synaptosomes prepared with or without detergent reveal different lipid and protein domains, *Brain Res. 962*, 144−150.
38. Pike, L. J., Han, X., Chung, K.-N., and Gross, R. W. (2002) Lipid rafts are enriched in arachidonic acid and plasmenylethanolamine and their composition is independent of caveolin-1 expression: A quantitative electrospray ionization/mass spectrometric analysis, *Biochemistry 41*, 2075−2088.
39. Gallegos, A. M., Atshaves, B. P., Storey, S., McIntosh, A., Petrescu, A. D., and Schroeder, F. (2001) Sterol carrier protein-2 expression alters plasma membrane lipid distribution and cholesterol dynamics, *Biochemistry 40*, 6493−6506.
40. Thomas, J. L., Holowka, D., Baird, B., and Webb, W. W. (1994) Large scale co-aggregation of fluorescent lipid probes with cell surface proteins, *J. Cell Biol. 125*, 795−802.
41. Schroeder, F., and Soler-Argilaga, C. (1983) Calcium Modulates Fatty Acid Dymanics in Rat Liver Plasma Membranes, *Eur. J. Biochem. 132*, 517−524.
42. Spink, C. H., Yeager, M., and Feigenson, G. W. (1990) Partitioning behavior of indocarbocyanine probes between coexisting gel and fluid phases in model membranes, *Biochim. Biophys. Acta 1023*, 25−33.
43. Florine-Casteel, K., and Feigenson, G. W. (1988) On the use of partition coefficients to characterize the distribution of fluorescent membrane probes between coexisting gel and fluid lipid phases: An analysis of the partition behavior of 1,6-diphenyl-1,3,5-hexatriene, *Biochim. Biophys. Acta 941*, 102−106.
44. London, E., and Brown, D. A. (2000) Insolubility of lipids in Triton X-100: Physical origin and relationship to sphingolipid/cholesterol membrane domains (rafts), *Biochim. Biophys. Acta 1508*, 182−195.
45. Simons, K., and Vaz, W. L. (2004) Model systems, lipid rafts, and cell membranes, *Annu. Rev. Biophys. Biomol. Struct. 33*, 269−295.
46. Sweet, W. D., and Schroeder, F. (1988) Polyunsaturated fatty acids alter sterol transbilayer domains in LM fibroblast plasma membrane, *FEBS Lett. 229*, 188−192.
47. Schroeder, F., Wood, W. G., and Kier, A. B. (2001) Lipid domains and biological membrane function, in *Cell Physiology Sourcebook: A molecular approach* (Sperelakis, N., Ed.) pp 81−94, Academic Press, New York.
48. Dudeja, P. K., Harig, J. M., Wali, R. K., Knaup, S. M., Ramaswamy, K., and Brasitus, T. A. (1991) Differential modulation of human small intestinal brush-border membrane hemileaflet fluidity affects leucine aminopeptidase activity and transport of D-glucose and L-glutamate, *Arch. Biochem. Biophys. 284*, 338−345.
49. Daleke, D. L., and Lyles, J. V. (2000) Identification and purification of aminophospholipid flippases, *Biochim. Biophys. Acta 1486*, 108−127.
50. Berthouex, P. M., and Brown, L. C. (1994) in *Statistics for Environmental Engineers* (Berthouex, P. M., and Brown, L. C., Eds.) pp 71−79, CRC Press, Boca Raton, FL.
51. Kavecansky, J., Joiner, C. H., and Schroeder, F. (1994) Erythrocyte membrane lateral sterol domains: A dehydroergosterol fluorescence polarization study, *Biochemistry 33*, 2880−2890.
52. Tabas, I. (1997) Free cholesterol-induced cytotoxicity, *Trends Cardiovasc. Med. 7*, 256−263.
53. Brown, D. A., and London, E. (1998) Functions of lipid rafts in biological membranes, *Annu. Rev. Cell Dev. Biol. 14*, 111−136.
54. Schroeder, R., London, E., and Brown, D. (1994) Interactions between saturated acyl chains confer detergent resistance on lipids and glycosylphosphatidylinositol (GPI)-anchored proteins: GPI-anchored proteins in liposomes and cells show similar behavior, *Proc. Natl. Acad. Sci. U.S.A. 91*, 12130−12134.
55. Radeva, G., and Sharom, F. J. (2004) Isolation and characterization of lipid rafts with different properties from RBL-2H3 (rat basophilic leukaemia) cells, *Biochem. J. 380*, 219−230.
56. Wood, G. W., Schroeder, F., Igbavboa, U., Avdulov, N. A., and Chochina, S. V. (2002) Brain membrane cholesterol domains, aging and amyloid β-peptides, *Neurobiol. Aging 23*, 685−694.
57. Sweet, W. D., and Schroeder, F. (1988) Lipid domains and enzyme activity, in *Advances in Membrane Fluidity: Lipid Domains and the Relationship to Membrane Function* (Aloia, R. C., Cirtain, C. C., and Gordon, L. M., Eds.) pp 17−42, Alan R. Liss, Inc., New York.
58. Schroeder, F., Frolov, A., Schoer, J., Gallegos, A., Atshaves, B. P., Stolowich, N. J., Scott, A. I., and Kier, A. B. (1998) Intracellular sterol binding proteins, cholesterol transport and membrane domains, in *Intracellular Cholesterol Trafficking* (Chang, T. Y., and Freeman, D. A., Eds.) pp 213−234, Kluwer Academic Publishers, Boston.
59. John, K., Kubelt, J., Muller, P., Wustner, D., and Herrmann, A. (2002) Rapid transbilayer movement of the fluorescent sterol dehydroergosterol in lipid membranes, *Biophys. J. 83*, 1525−1534.
60. Boesze-Battaglia, K., Clayton, S. T., and Schimmel, R. J. (1996) Cholesterol redistribution within human platelet plasma membrane: Evidence for a stimulus-dependent event, *Biochemistry 35*, 6664−6673.
61. Atshaves, B. P., Starodub, O., McIntosh, A. L., Roths, J. B., Kier, A. B., and Schroeder, F. (2000) Sterol carrier protein-2 alters HDL-mediated cholesterol efflux, *J. Biol. Chem. 275*, 36852−36861.
62. Fuchs, M., Hafer, A., Muench, C., Kannenberg, F., Teichmann, S., Scheibner, J., Stange, E. F., and Seedorf, U. (2001) Disruption of the sterol carrier protein 2 gene in mice impairs biliary lipid and hepatic cholesterol metabolism, *J. Biol. Chem. 276*, 48058−48065.
63. Schroeder, F., Gallegos, A. M., Atshaves, B. P., McIntosh, A., Petrescu, A. D., Huang, H., Chao, H., Yang, H., Frolov, A., and Kier, A. B. (2001) Recent advances in membrane microdomains: Rafts, caveolae and intracellular cholesterol trafficking, *Exp. Biol. Med. 226*, 873−890.

BI0602720